LA-UR-10- 10-00459

Approved for public release; distribution is unlimited.

Title: A Variable Density Atmosphere Model for MCNP6

Author(s): Stepan G. Mashnik

Intended for: Distribution

Los Alamos
NATIONAL LABORATORY
research note
X-Computational Physics, XCP
Monte Carlo Codes, XCP-3

To/MS: Distribution
From/MS: S. G. Mashnik, XCP-3, MS A143
Phone/FAX: 7-9946/5-4479
Email: mashnik@lanl.gov
Symbol: X-3-RN(U)09-013, LA-UR-10-xxxx
Date: Setpember 16, 2009

A Variable Density Atmosphere Model for MCNP6

Abstract

This Research Note presents a summary and progress report on a modification of the transport code MCNP6 to allow a capability of accounting variation of the air density with the altitude (continuously varying density cell capability).

1. Introduction

MCNP6, just like other transport codes, uses the density of simulated objects to calculate the mean free path of the traced particles in the media. The standard version of MCNP6 assumes that the density of a simulated cell, ρ, is approximately constant, that allows us to estimate the mean free path of a neutral particle in the media, λ, assuming that we know the total "microscopic" cross section for the interaction of particle with the material, σ, and also assuming that this cross section does not vary within the cell, namely, $\lambda = 1/\sigma\rho$.

However, there are cases (see, e.g., [1]) when these assumptions do not fulfill well, causing difficulties in applying the standard MCNP6 to such problems. So, because the density of atmosphere varies nearly exponentially with the altitude, a very large number of cells is required to simulate interaction of radiation with a large region of the atmosphere. This imposes limitations to the computing time, to the needed memory, and to the accuracy of final results.

If a variable density atmospheric model could be implemented in MCNP6, an improvement over the standard version could be achieved. We could increase the dimensions of our geometry and could decrease the run time of our problem, increasing meanwhile the accuracy of the simulated results and making the input simpler and easier to write.

Several different approaches can be used to address problems where the density of the material and/or the cross-sections vary significantly for the geometry we simulate. As was noted by Brown and Martin [1], the first method people usually use when simulating media with strongly varying cross-sections or/and densities is *sub-stepping*, i.e., breaking the flight path into short segments within which the cross-section or/and the density is assumed constant [2]. In our case of simulating the atmosphere, this would mean simply using more cells, that could lead to very expensive calculations; so, we have to find another approach for our problem.

Another common approach reviewed briefly in [1] is the so-called *delta-tracking* method [3]-[6]. This technique dates back to 1960s and is also called *pseudo-scattering*, *hole-tracking*, *Woodcock tracking*, or *self-scattering*.

A third approach, developed by Brown and Martin with co-authors is the so-called *direct method* [1, 7, 8]. This method involves random sampling followed by numerical solutions via Newton integration.

Finally, a forth method, used widely in atmospheric radiation problems is the so-called *Mass Integral Scaling* approach [9]-[15]. Here, we follow this last method, described briefly in the next section, to modify MCNP6 for accounting for a variable density atmosphere.

2. Mass Integral Scaling Approach

The Mass Integral Scaling (MIS) technique is widely used to study the transport of radiation in homogeneous media, e.g., by the user-oriented mass scaling codes like ATR [13], CDR [14], and SMAUG [15]. For application to the atmospheric radiation transport problems, the MIS law can be stated as follows [9]: **In an infinite homogeneous medium with an isotropic point source, the $4\pi R^2$ fluence (time integrated flux) or dose is a function only of ρR, the mass per unit area between the source and a receiver.** In homogeneous air, ρR, is equal to the "mass range" or "areal density". In a general case, "mass range" is the integral of the density along a straight line between the source and a receiver point. In constant density homogeneous air, **mass range** is simply the product of the density and the slant range between the source and the receiver, as mentioned above. In 1956, Zerby [10] presented a simple derivation of the mass scaling law using the Boltzmann transport equation. Shultstad had shown later [9] that the scaling law can be derived from the diffusion equation in a similar manner and under the exact same set of assumptions used by Zerby [10].

To clarify how mass scaling is applied in homogeneous air and how can it be extended to a variable density air, let's consider the following example [9]. If identical isotropic point sources are placed in two infinite homogeneous air media (medium A and medium B), and if two slant ranges, R_A and R_B, in the two media are related by

$$\rho_A R_A = \rho_B R_B \ , \tag{1}$$

where ρ is the density in the respective media, then, as shown by Shultstad [9], the energy dependent fluence, $F(R, E)$, at ranges R_a and R_B are related as

$$4\pi R_A^2 F(R_A, E) = 4\pi R_B^2 F(R_B, E) \ . \tag{2}$$

If the atmosphere were homogeneous, the mass scaling law could be rigorously applied, without error, to quickly compute environments under a wide variety of scenarios. Unfortunately, this is not exactly the case: The density in the U.S. Standard Atmosphere [16], is not constant but decreases in an exponential-like fashion with altitude. The application of the mass scaling law in variable density atmosphere requires a careful definition of mass range. The mass range in this atmosphere is defined to be the mass integral, $< \rho R >$, which can be written as

$$< \rho_B R_B >= \int_0^{R_B} \rho(z) dR_B \ , \tag{3}$$

and is also sometime referred to as the "areal density".

To show how the mass scaling law is applied in variable density air, assume that medium A is homogeneous air and that medium B is the U.S. Standard Atmosphere [16]. The mass integral scaling approximation assumes that if the mass range between a source and receiver in variable density air is equal to the mass range in homogeneous air

$$\rho_A R_A = \int_0^{R_B} \rho(z) dR_B \ , \tag{4}$$

then the $4\pi R^2$ fluence will be the same, as given by Eq. (2).

So, the fundamental assumptions made in models using mass integral scaling approximation is that homogeneous air transport results can be mass integral scaled to generate a radiation environment intended to reflect the near-exponential nature of the U.S. Standard Atmosphere [16]. Since the mass scaling law was derived [10] under the assumption of an infinite homogeneous media, it should be clear that it becomes an approximation when expended to variable density air. As shown by Shultstard [9], the effects of leakage, mass distribution, and the air/ground interface can all produce some perturbations in the mass integral scaled dose in variable density air.

3. Test-Problems with Unmodified MCNP6

Since the MIS approach was used earlier by Monti [11, 12] to solve similar problems with MCNP3B, it is natural to compare our results with similar results by Monti. Before starting to implement MIS into MCNP6, we need to run several test-problems with the standard, unmodified MCNP6 using a large number of atmosphere cells, similar to the test-problems addressed by Monti [11] and earlier, by Culp et al. [17]. Most important, we need such benchmarking results by unmodified MCNP6 to make sure that the modified here MCNP6 provides results in good agreement with them.

We chose for our unmodified MCNP6 several test-problems with a geometry very similar to the one used by Culp et al. [17] and by Monti [11]. Note that we may expect a little difference between our unmodified calculation results and the ones published by Culp et al. [17] and by Monti [11] because we use now the modern MCNP6 with newer data libraries available to us, while Culp et al. and Monti used the older MCNP3B with some older data libraries available to them almost twenty years ago.

An example of an input used in our unmodified MCNP6 calculations is presented in Appendix 1. The geometry of the problems with an isotropic fission source of neutrons at 40.05 km (see Appendix 1) is shown in Fig. 1.

To tally the energy deposition at a source co-altitude, we specify in our geometry 15 ring-form cells with their center at an altitude of 42.5 km and with their mean radius values R from 1.25 km to 95 km, respectively (see Fig. 1). To tally the neutron fluence and the fluence of secondary photons at a source co-altitude, we use 19 ring detectors at 40 km altitude with their radius values from 1 km to 100 km, respectively (see Appendix 1).

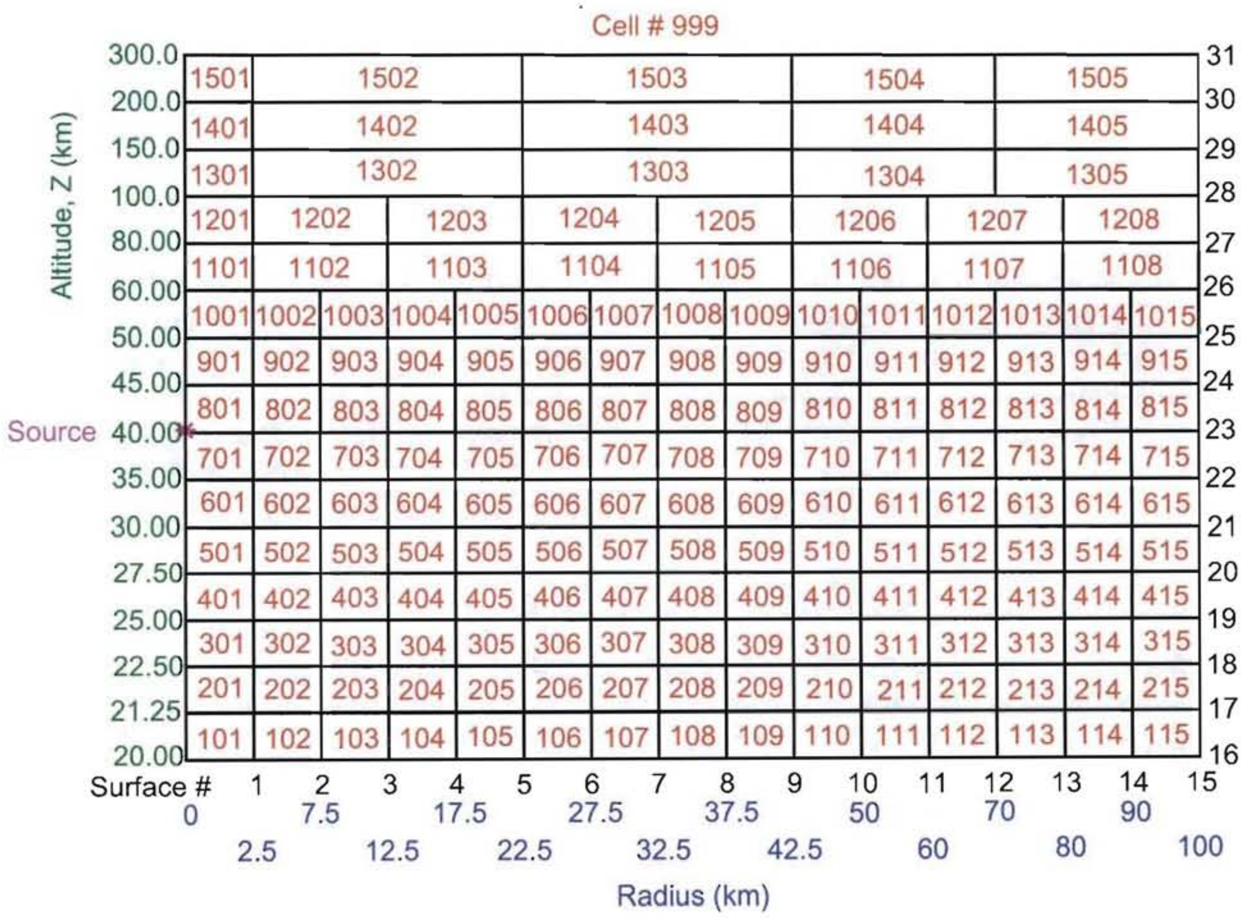

Figure 1: Spatial cell geometry for the High Altitude (above 20 km) test problems with the unmodified MCNP6.

Examples of our neutron fluence test-results by the unmodified MCNP6 together with corresponding results by Monti [11] are shown in Fig. 2; mean neutron energy deposition results are compared in Fig. 3 with Culp et al. [17] results by the unmodified MCNP3B; an example of secondary photon fluence is compared in Fig. 4 with with results by Monti with a modification of MCNP3B [11].

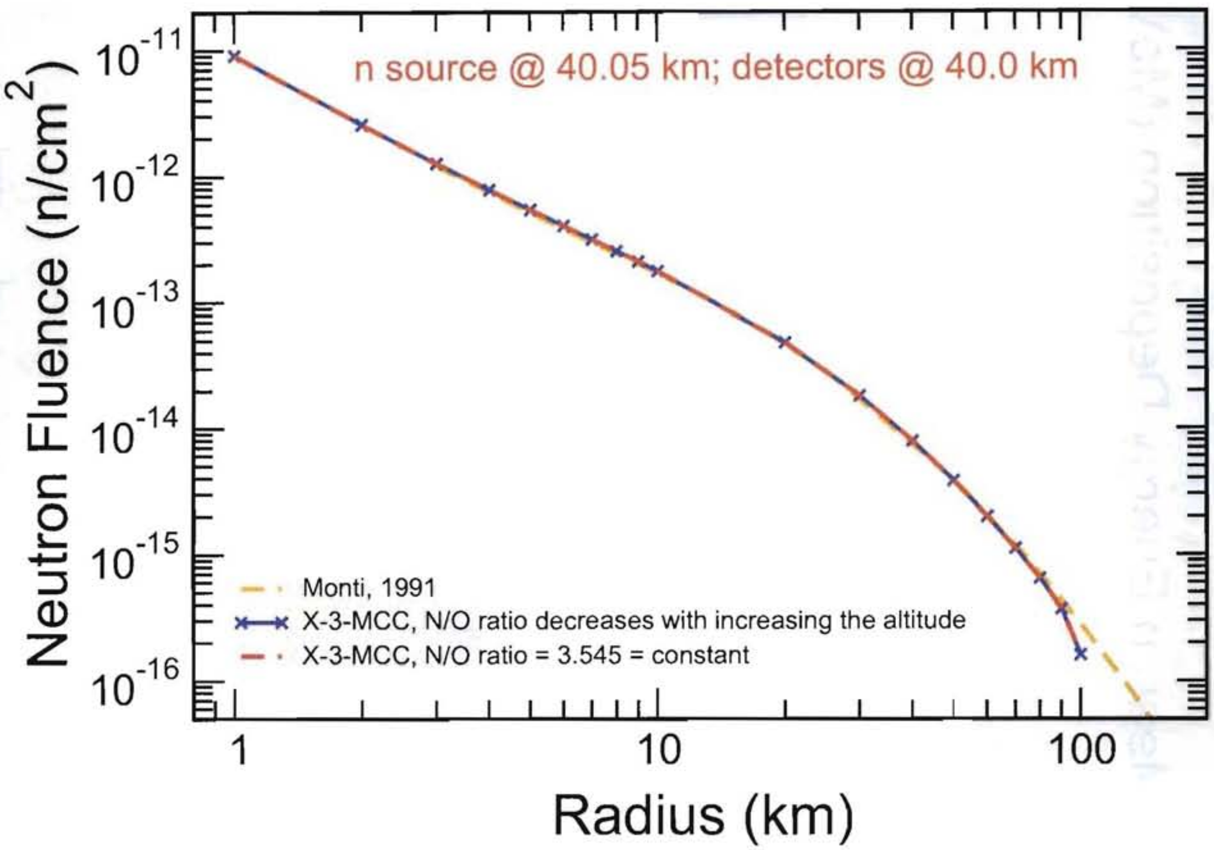

Figure 2: Neutron fluence at 40 km from a source at 40.05 km vs. radius (slant range) calculated with the standard, unmodified MCNP6 for the geometry shown on Fig. 1 using a Nitrogen-to-Oxygen ratio for the air decreasing with the increase of the altitude according to the U.S. Standard Atmosphere Tables, 1976 [16] (solid blue line) and using a constant, sea-level, N/O ratio (red dashed line) compared with results by Monti with a modification of MCNP3B [11] (orange dashed line).

We see that our results by the unmodified MCNP6 agree very well with the corresponding results by Culp et al. [17] and by Monti [11] for all three characteristics shown in Figs. 2-4, for almost the entire geometry considered. A little difference can be observed only for the radius R=100 km, but it is probably because this point is just on the very border of our geometry: to get reliable results for this point, we would need to enlarge our geometry, adding more cells, so that contributions from re-scattering back from larger values of R to this point are accounted.

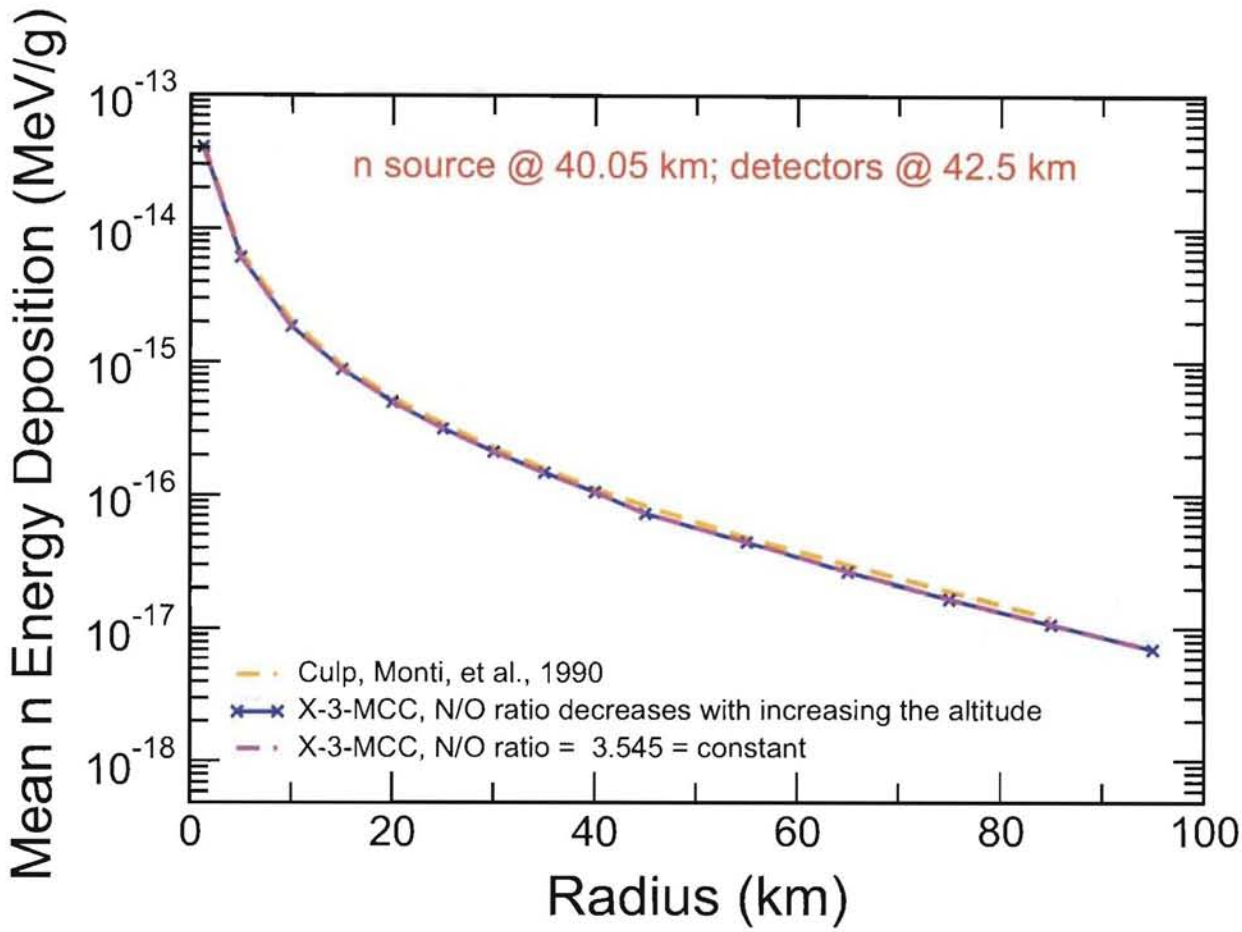

Figure 3: Mean neutron energy deposition at 42.5 km from a source at 40.05 km vs. radius (slant range) calculated with the standard, unmodified MCNP6 for the geometry shown on Fig. 3 using a Nitrogen-to-Oxygen ratio for the air decreasing with the increase of the altitude according to the U.S. Standard Atmosphere Tables, 1976 [16] (solid blue line) and using a constant, sea-level, N/O ratio (red dashed line) compared with unmodified MCNP3B results by Culp et al., [17] (orange dashed line.

The MIS method applied to the atmospheric radiation transport problems assumes initially that the density of all air cells is equal to the air density at the sea-level, with fixed ratios for different isotopes in the air, and only later, simulating the mean free path of radiation through the air, accounts that the density of the air actually varies with the altitude, still using fixed ratios for different air nuclides at all altitudes (see details, e.g., in [11]). Because of these assumptions, it is necessary to check how the unmodified MCNP6 results depend on the ratios for different isotopes of the air we use in our calculations.

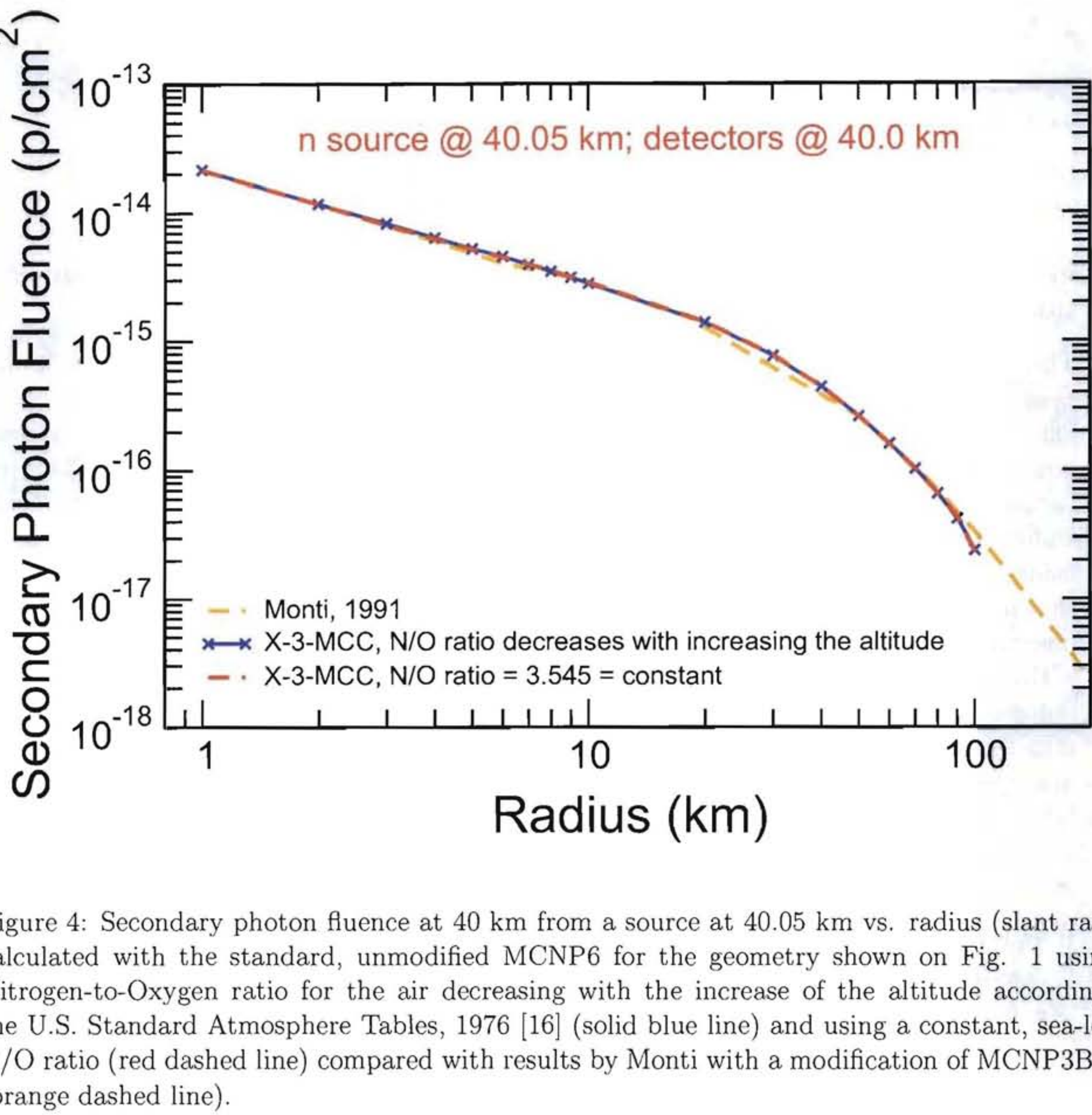

Figure 4: Secondary photon fluence at 40 km from a source at 40.05 km vs. radius (slant range) calculated with the standard, unmodified MCNP6 for the geometry shown on Fig. 1 using a Nitrogen-to-Oxygen ratio for the air decreasing with the increase of the altitude according to the U.S. Standard Atmosphere Tables, 1976 [16] (solid blue line) and using a constant, sea-level, N/O ratio (red dashed line) compared with results by Monti with a modification of MCNP3B [11] (orange dashed line).

For all our unmodified MCNP6 test problems, we performed calculations using a real Nitrogen-to-Oxygen ratio, decreasing with increasing the altitude according to the U.S. Standard Atmosphere Tables, 1976 [16], as well as calculations with a fixed N/O ratio equal to the sea-level value of 3.545. Results presented in Figs. 2-4 show that values calculated using decreasing N/O ratio with increasing the altitude are very near to the results obtained using a fixed, sea-level, N/O ratio for all cells, proving that the MIS approach of using fixed ratios for different isotopes of the air is good enough and does not affect significantly the final results.

4. Modification of MCNP6

At altitudes below ~ 110 km, the density of the air decreases nearly exponentially with increasing the altitude, and the variation of the air density can be approximated as:

$$\rho(Z) = \rho_0 \exp\left(-\frac{Z}{7}\right) , \tag{5}$$

where $\rho(Z)$ and ρ_0 are the densities of air at the Z-altitude and sea-level, respectively, and the altitude Z is given in [km].

The 7 km scale height factor in Eq. (5) represents the vertical distance required for the air density to decrease by a factor of e. This model of the atmosphere is often referred to as the "7 km" atmosphere. If this model was exact and the variation of the atmosphere density was described exactly by Eq. (5), it would be much easier to modify MCNP6 to account for a variable density, as all the integrals could be taken analytically for the entire atmosphere. Unfortunately, as can be seen from Fig. 5, the real atmospheric density cannot be represented by using density altitude bins which use a single constant density scale height factor of 7 km. As shown in [11], if we approximate the variation of the atmosphere density using a series of piecewise-constant spatial grids to represent $\rho(r)$, a continuously variable exponential function within each region, each with a characteristic scale height factor, would be more accurate for representing the variation of the air density as a function of altitude. Let us mention beforehand that this approximation simplify significantly our modification of MCNP6: We input a set of atmosphere densities at a number of points along an input line understanding that the scale height factor is different in different atmosphere regions, but assuming that it can be considered as constant inside any given region; This allows us to calculate the mass integrals analytically in every given region.

If we approximate the variation of air density as piecewise exponential and divide the atmosphere into vertical regions, then curve-fits for the density variation have the following form (for $Z_i \leq Z \leq Z_{i+1}$):

$$\rho(Z) = \rho(Z_i) \exp\left[-\frac{(Z - Z_i)}{S_i}\right] , \tag{6}$$

where $\rho(Z)$ is the density at a specified Z altitude, $\rho(Z_i)$ is the density at the base altitude of the ith region, S_i is the density scale height factor for the ith region, while Z_i and $\rho(Z_i)$ are input values. Using for Z the value of Z_{i+1} defined by the input, Eq. (6) can be easily solved against S_i:

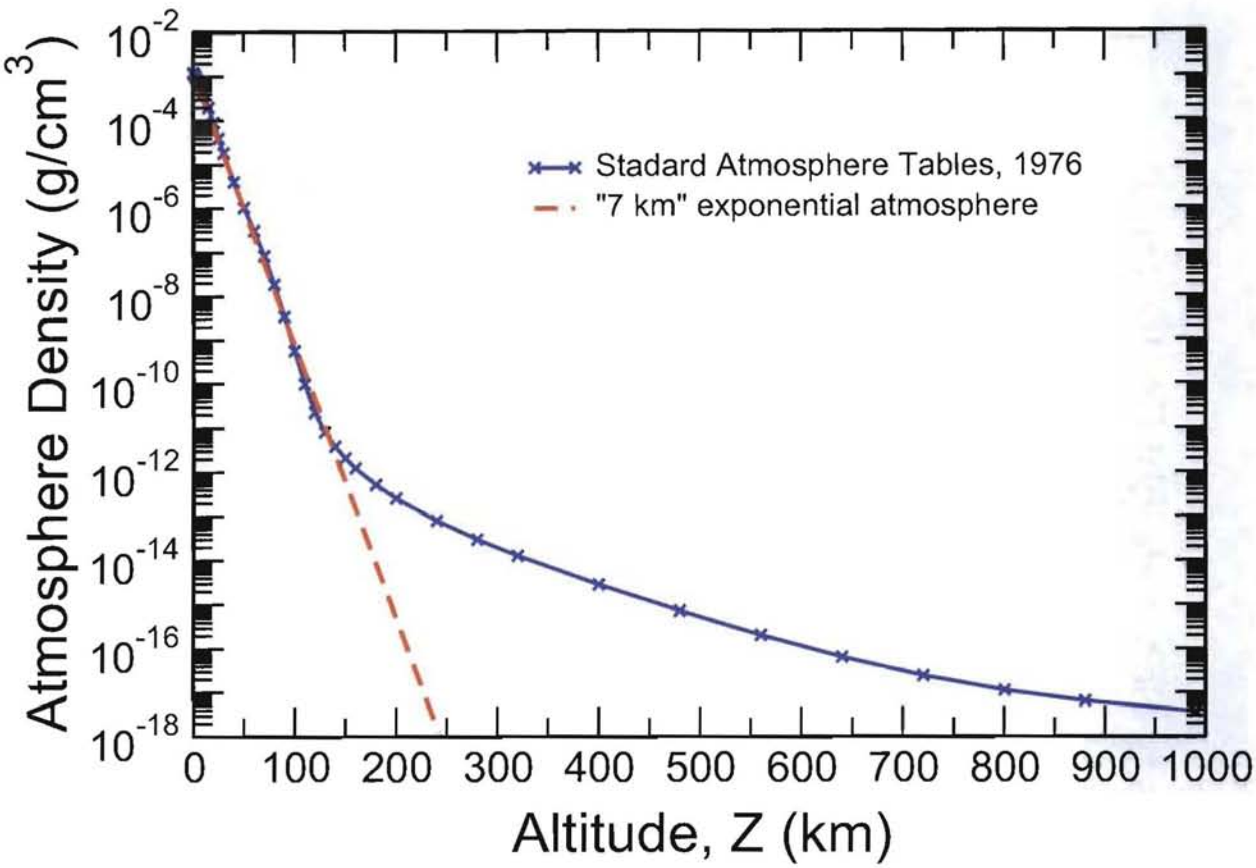

Figure 5: Air density vs. geometric altitude from the U.S. Standard Atmosphere Tables, 1976 [16] (blue solid line) compared with the "7 km" approximation (red dashed line).

$$S_i = \frac{(Z_i - Z_{i+1})}{\ln[\rho(Z_{i+1})/\rho(Z_i)]} \ , \tag{7}$$

allowing us to determine S_i from the input values of $\rho(Z_i)$ and Z_i.

Calculated according to Eq. (7) density scale height factors S_i for a set of Z_i with $\rho(Z_i)$ from the U.S. Standard Atmosphere Tables, 1976 [16] are compared in Fig. 6 with values by Monti [11]. We see a perfect agreement between our and Monti values of S_i.

In order to perform MCNP6 calculations in a variable density atmosphere, it is necessary to know the integrated mass density ("mass-integral") values as a function of altitude $M_I(Z)$ (two simple auxiliary routines, **function masi** and **function miz** were written to calculate mass integrals between two points in space).

$$M_I(Z) \equiv \int_0^Z \rho(Z)dZ = M_I(Z_i) + \int_{Z_i}^Z \rho(Z)\exp\left[-\frac{(Z-Z_i)}{S_i}\right]dZ\ . \tag{8}$$

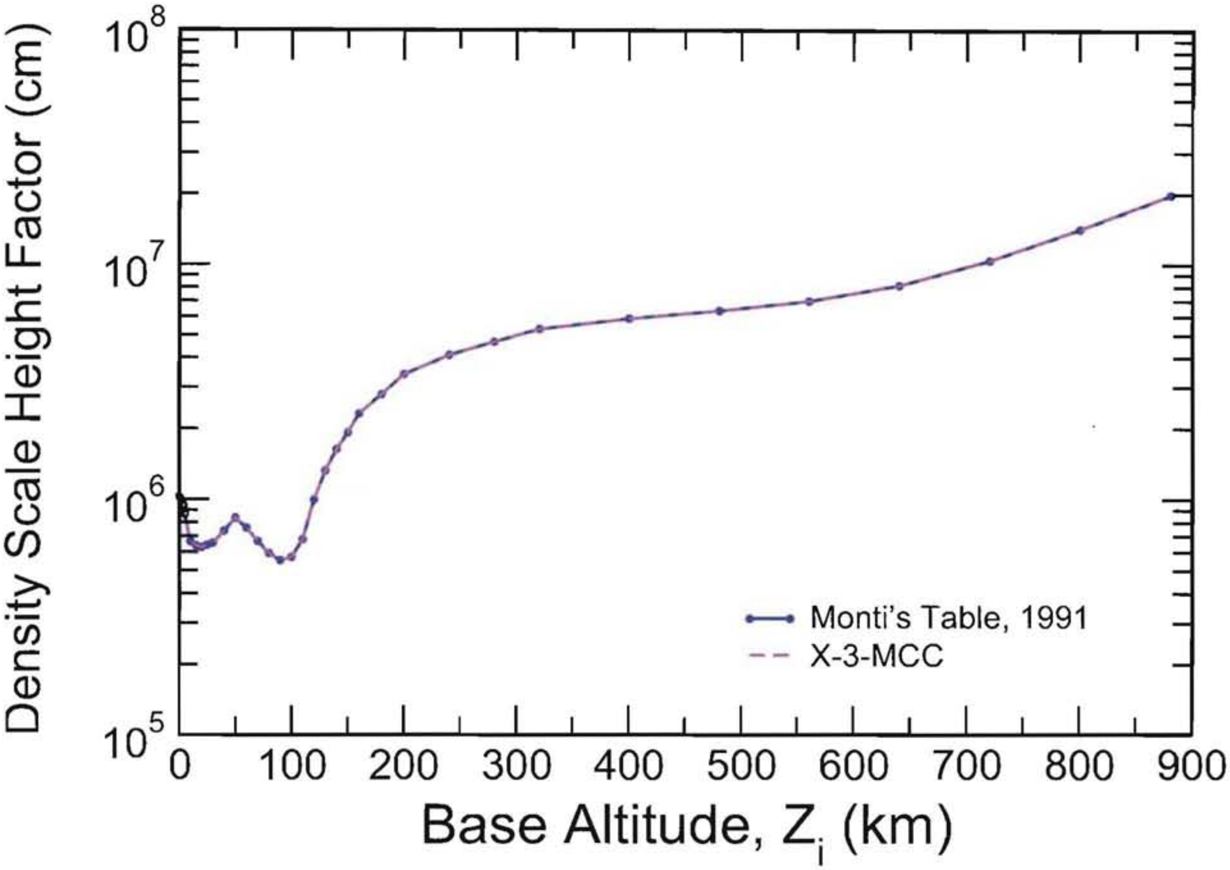

Figure 6: Calculated here density scale height factor for the U.S. Standard Atmosphere Tables, 1976 [16] (red dashed line) compared with values by Monti [11] (blue solid line).

To simplify our work, we use for the mass integrals $M_I(Z)$ the same altitude regions i inputted for the density data. In this case, we can calculate the mass integral in each region by integrating Eq. (8) over the altitude. Keeping in mind that S_i was already defined by Eq. (7) and was assumed to be constant inside each region, the integral (8) can be easily calculated analytically for each region:

$$M_I(Z) = M_I(Z_i) + \rho(Z_i)S_i\left[1 - \exp\left(-\frac{(Z-Z_i)}{S_i}\right)\right]\ . \tag{9}$$

This point was not understood by Monti [11], forcing him to calculate initially the integral (8) numerically for the entire atmosphere with a special QuickBasic program he wrote for this purpose. Then, from the found values of $M_I(Z)$, he had to calculate the scale factors S_i for every region i he used. This fact led Monti [11] to so called *mass-integral scale height factors* S_i he tabulated in Tab. 3 of Ref. [11] with slightly different values from the ones he found earlier for air density from Eq. (6), he called *density scale height factors* and tabulated in Tab. 2 of Ref. [11].

Let us note that Monti values for the *mass-integral scale height factors* S_i differ slightly also from our values, which must be identical to the *density scale height factors*, calculated using Eq. (7) and shown in Fig. 6. In addition, although our *density scale height factors* S_i shown in Fig. 6 agree very well with the corresponding values by Monti, so that the two lines lines shown in the figure practically coincide within the scale of the plot, the exact numerical values do actually also differ a little. This is why we decided to provide for users of the current variable density modification of MCNP6 two options: A) A possibility of using the Monti parameters for both *the density scale height factors* and *mass-integral scale height factors*; this option works well, its parameters are based on the whole atmosphere, but are fixed and valid only for the atmosphere of our Earth, and do not depend on densities the users want to employ in their problems. B) A more general option of using our X-3-MCC method, which calculates the *density scale height factors* with Eq. (7) from the inputted values of the densities at a number of locations inputed for each problem. In the case of the atmosphere of our Earth, our method provides results very close to the method of using the Monti parameters. But our X-3-MCC method is more universal and not restricted to only the Earth atmosphere: Users are allowed to enter in their input densities at a number of locations for arbitrary problems, e.g., for the atmosphere of the Moon or Mars, and our method is expected to work properly for arbitrary cases.

Fig. 7 shows the mass integral calculated according to Eq. (9) with S_i defined by Eq. (7) we use in our modified MCNP6 (dashed red line) compared with Monti values of $M_I(Z)$ tabulated in Tab. 3 of Ref. [11] (solid blue line), as well as compared with values calculated according to Eq. (9) but using the so-called *mass-integral scale height factors* S_i provided by Monti in his Tab. 3 of Ref. [11] (dashed green line). As expected, we see a very good agreement between our and Monti values of $M_I(Z)$, but we may observe a tiny difference at altitudes above ~ 20 km between our values and the ones calculated using the so-called *mass-integral scale height factors* by Monti.

Inverting Eq. (9) results in the following expression which calculates the altitude given a mass-integral

$$Z = Z_i - S_i \ln\left[1 + \frac{(M_I(Z_i) - M_I(Z))}{\rho(Z_i) S_i}\right] . \tag{10}$$

Eq. (10) is used in an auxiliary **function zmas** of the modified MCNP6 to calculate the collision altitude, after the mass-integral at the collision altitude is calculated with an auxiliary **function miz** in the user-written **subroutine eqdist**. Note that the mass-integral at 990 km calculated with Eq. (9) was found to be equal to 1035.635131402448 g/cm^2, when using the

Monti density and mass-integral scale height factors, and equal to 1031.891228951410 g/cm^2, when calculated with the X-3-MCC method as described above. These values are defined as the upper limit of the atmospheric model, i.e., as the mass-integral at infinity, and are assigned in **subroutine vardens_parameters_setup** to the real variable *infinity_mass_integral* used further in the modified **subroutine transm**.

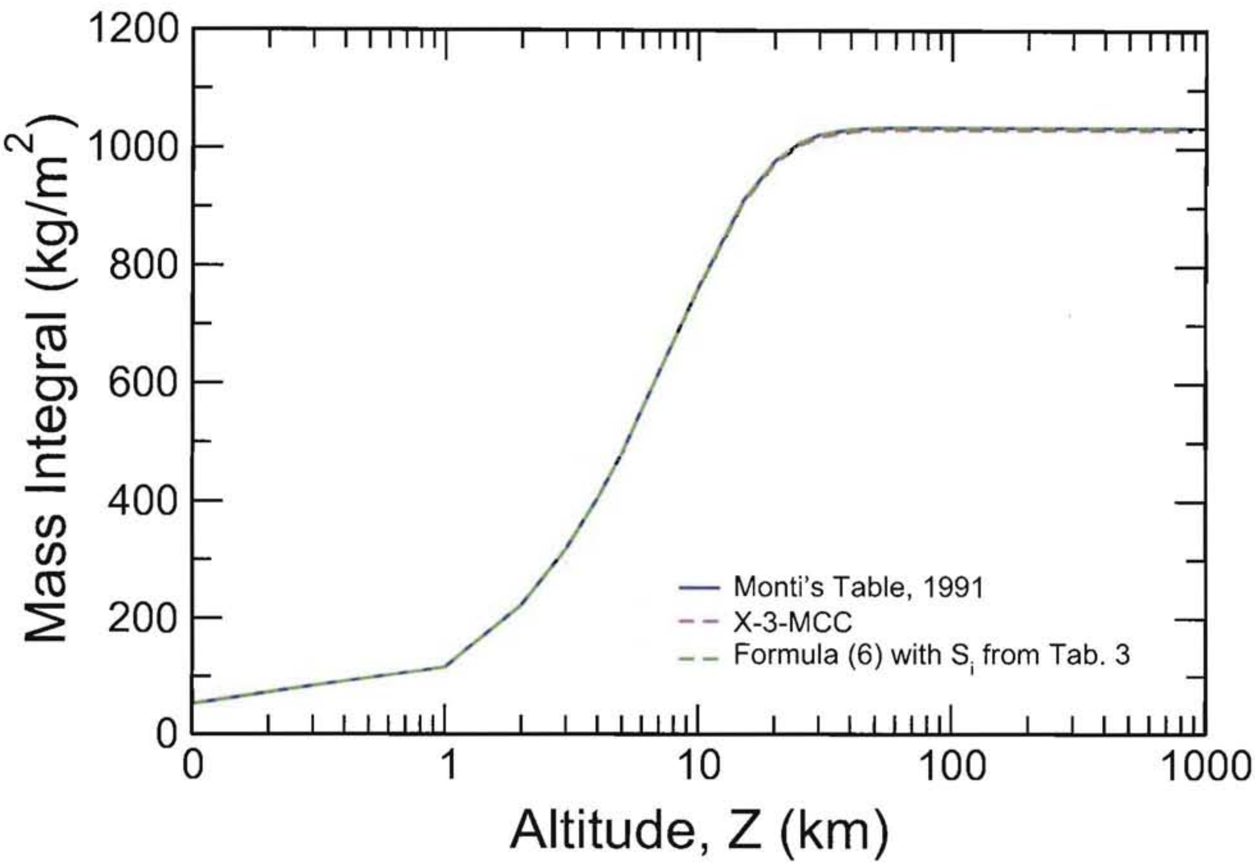

Figure 7: Calculated here mass integral as a function of geometric altitude for a polar angle of zero degrees (red dashed line) compared with tabulated values by Monti (blue solid line) and with calculations using Eq. (9) with so-called "mass scale height factors" from Tab. 3 of Ref. [11] (dashed green line).

Before starting to modify **subroutine history_neutral_low** (**hstory.F90**), the main routine running a history of a neutral particle flow in MCNP6, we modify a little **subroutine nextit** (**nextit.F90**) processing the next input item to set the densities of all air cells equal to the sea-level value $\rho_0 = 1.225\text{e-}3$ [g/cm^3]: In the standard, unmodified version, MCNP6 computes density-dependent parameters using a discrete cell density defined in the input. In the modified version, the variation of air density is continuous, and a constant density spatial mesh in the vertical direction is no longer needed; cells are needed only to calculate tallies, using splitting or Russian roulette.

The distance to next collision of a neutral particle, l (coded as *pmf* in MCNP6), is simulated in **subroutine history_neutral_low** based on the "microscopic" cross sections σ (*totm*) in the cell and the atomic density in the cell, ρ (*rho(icl)*)

$$l = -\frac{1}{\lambda} \ln \xi \ , \tag{11}$$

where ξ is a random number uniformly distributed on (0,1) and the mean free path $\lambda = 1/\sigma\rho$. Since l depends on ρ, which was already redefined in **subroutine nextit** to be the air density at the sea-level, it is necessary to correct it for a variable density atmosphere. **Subroutine eqdist**, called from **subroutine history_neutral_low** , was written to calculate the correct distance to collision based on input from **subroutine history_neutral_low**, i.e., current particle altitude Z (*zzz*), Z-direction cosine $\cos\phi$ (*www*), and distance to next collision based on a sea-level homogeneous atmosphere l_0 (*mpf*).

The mass-integral along the particle path in a homogeneous sea-level atmosphere is calculated as $M_{IPDH} = \rho_0 l_0$. This calculation is performed in **function dmi**.

Once the scale height region has been determined by the input and S_i calculated with Eq. (7) in **subroutine vardens_parameters_setup**, the cumulative mass-integral, M_{ICA}, at the current particle altitude, Z_0, can be computed using Eq. (9). This calculation is done in **function masi**.

Though the next collision altitude, Z_c, is still unknown, the values of M_{IPDH}, M_{ICA}, and the Z-direction cosine, $\cos\phi$ (coded as *w0* in **subroutine eqdist** and in **function miz**), can be used to calculate the required cumulative mass-integral M_{ICP} at the next collision altitude Z_c as $M_{ICP} = M_{ICA} + M_{IPDH} \times \cos\phi$. This calculation is performed by calling **function miz**.

At this point, a check is made to compare the computed cumulative mass-integral at the next collision altitude, M_{ICP}, with the mass-integral at infinity, M_{IINF}, defined as described above. If $M_{ICP} > M_{IINF}$, then **subroutine eqdist** is exited and l (*pmf*) is set to *huge_float* = 1.0e+36 (a very large number used by MCNP6 as a stand-in for infinity), effectively eliminating any future collisions along the current particle track. If $M_{ICP} \leq M_{IINF}$, then **function zmas** calculates the next collision altitude, Z_c, using Eq. (10).

For cases where the Z-direction cosine, $\cos\phi$, becomes very small (nearly co-altitude relative to the current particle position), the change in density is very small along the particle path. Therefore, the average density between the current altitude and the collision altitude is used. The air densities are calculated in such cases by calling **function dnty**.

Finally, the distance to collision, l (coded as *pmf* in **subroutine history_neutral_low** and as *edst* in **subroutine eqdist**), corrected for a variable density atmosphere, is computed by calling

function equivdist. **Function equivdist** accepts as inputs the next collision altitude, Z_c, the current particle altitude, Z_0, the Z-direction cosine, $\cos\phi$, the mass-integral along the particle direction in a homogeneous sea-level atmosphere, M_{IPDH}, and the densities (calculated only if $\cos\phi$ is small). For cases where $\cos\phi$ is not small, the corrected distance to next collision is equal to: $l = (Z_c - Z_0)/\cos\phi$. For cases where $\cos\phi$ is small, the density is nearly constant along the particle path, hence the corresponding distance to collision is given by: $l = M_{IPDH}/[(\rho_c + \rho_p)/2]$, where ρ_c and ρ_p are air densities at the next collision and current particle altitudes, respectively.

Contributions to a detector are made at every source or collision point by creating and transporting a pseudo-particle directly to the detector. The total transmission to the detector depends on the exponential attenuation through the medium, which represents the total attenuation of the radiation by the atmosphere, $\exp(-N_{mpf})$, along the particle path over a given number of mean free paths, N_{mfp} (coded as *amfp* in MCNP6). As the mean free path, $\lambda = 1/\sigma\rho$, and its reciprocal, $\sigma\rho$, called as *"macroscopic cross section"* in the cell (coded as *ple* in MCNP6) are calculated initially for a sea-level homogeneous atmosphere in the modified version of the code, it is necessary to correct them for a variable density atmosphere calling **subroutine eqdist** from **subroutine transm**, which calculates the attenuation, in the same manner and using the same formulas as is done while running a history of a neutral particle by **subroutine history_neutral_low**, as described above. A flag is set prior to calling **subroutine eqdist** in **subroutine transm** to indicate the origin of the calling statement, either **subroutine history_neutral_low** or **subroutine transm**.

As mentioned above, the current variable density modification of MCNP6 allows users to chose either Monti parameters or the X-3-MCC method to calculate the scale height factors. Actually, the users of the modified MCNP6 have also the option to calculate their problem with the standard MCNP6, without taking into account the current modifications. The choice of the version of MCNP6 the users like to use in their calculations is made as following: 1) If the users of the modified MCNP6 use in their inputs only old, standard MCNP6 input cards, like the ones shown in Appendix 1, calculations will be made with the standard version of MCNP6; 2) If the users add to their input a new data card called *vard*, without any information on it (i.e., an empty *vard* card, with only the word *vard* on it, as we have in the case of the empty *print* input card, with only the word *print* on it), the modified MCNP6 will use the Monti values for the density and mass-integral scale height factors, independently of the densities inputted for the cells of the problem. 3) To chose the X-3-MCC method, the users have to add two new input data cards (see Appendix 2): A) *vard* card with values for the three cosine directions, *vdalpha* $= \cos\alpha$, *vdbeta* $= \cos\beta$, and *vdgamma* $= \cos\gamma$ determining the direction of a line where a number of densities are inputted at corresponding positions; B) *varda* card with pairs of values for the distances from the sea-level *l(i)* and densities $\rho(i)$ at a number of positions along the line defined by the cosine directions *vdalpha, vdbeta* , and *vdgamma* inputted with the input card *vard.* The format of *vdalpha, vdbeta, vdgamma*, and of *l(i)* and $\rho(i)$ on the *vard* and *varda* cards is arbitrary; Appendix 2 shows an example of *vard* and *varda* input cards.

To add the two new MCNP6 input cards, *vard* and *verda*, we had to modify **module mcnp_input**, **subroutine newcd1**, **subroutine nxtit1**, **subroutine nextit**, and **module fixcom**. As the dimension of arrays for inputted positions and densities, $l(i)$ and $\rho(i)$, and respectively of arrays with altitudes and with corresponding scale factors is chosen by users according to the inputted data on the *varda* card and is not known in advance, we had also to modify **subroutine dyn_allocate** of the package **setdas.F90** and to write a new auxiliary **subroutine varden_setup** to allocate/deallocate dynamically memory for these arrays depending on the input.

We have tested the modified MCNP6 on several test problems using a geometry allowing us to calculated characteristics as calculated above with the unmodified code, to be able to test results by the modified version against the ones by the standard MCNP6 shown in Figs. 2-4.

The geometry used for the test-problems with the modified MCNP6 is shown in Fig. 8, with an example of the input shown in Appendix 2. Note that the geometry in the modified MCNP6 can be much simpler, with much fewer cells. In fact, in the example of the input shown in Appendix 2, we had to include cells # 401-423 in the modified tests only to calculate the energy deposition of neutrons at a source altitude of 40 km as a function if the radius, to compare these results with similar ones by the unmodified version shown in Fig. 3. As in the case of unmodified tests, the neutron and secondary photon fluence is calculated using ring detectors at 40 km altitude.

Results by the modified MCNP6 for the neutron fluence, mean neutron energy deposition, and for secondary photon fluence are presented in Figs. 9-11, respectively. We show in these figures results obtained with all three mentioned above options allowed by the modified MCNP6: 1) Without the new *vard* input cards, i.e., calculated with the standard version of MCNP6, without considering the new variable density capabilities and using the "extended" geometry shown in Fig. 1, with 182 ("many") cells (red dashed lines); 2) calculation with the variable density version using the fixed Monti parameters for the density and mass-integral scale factors, using the "reduced" geometry shown in Fig. 8, with only 29 ("few") cells (solid green lines); 3) calculations with the variable density version using the more universal X-3-MCC method, for the "reduced" geometry with "few" cells (black dashed lines). In the legends of these figures, we show also the time needed to run in sequential mode 10^6 histories (nsp = 1000000) on a single Yellowrail node of the Roadrunner supercomputer of LANL.

One can see a very good agreement between results by these three different sets of calculations. In addition, that may be very important in applications with complex geometries, the variable density version using only a "few" cells requires several times less computing time in comparison with the standard MCNP6 with "many" cells.

4. Summary

A modification of the transport code MCNP6 to allow using variation of the air density with the altitude (continuously varying density cell capability) using the mass-integral scaling approach was made. The modified version of the code was tested against results by the standard, unmodified MCNP6 and against similar results by other authors. A very good agreement was obtained, proving that the mass-integral scaling law is a good approximation, and the model was properly incorporated into the modified MCNP6. The variable density modification of MCNP6 allows us to save computing time, providing meanwhile reliable results in a very good agreement with corresponding results by the unmodified, standard MCNP6.

Acknowledgment

I am grateful to Drs. Roger Martz, Grady Hughes, Richard Prael, Forrest Brown, and Jeremy Sweezy for numerous useful discussions and kind help.

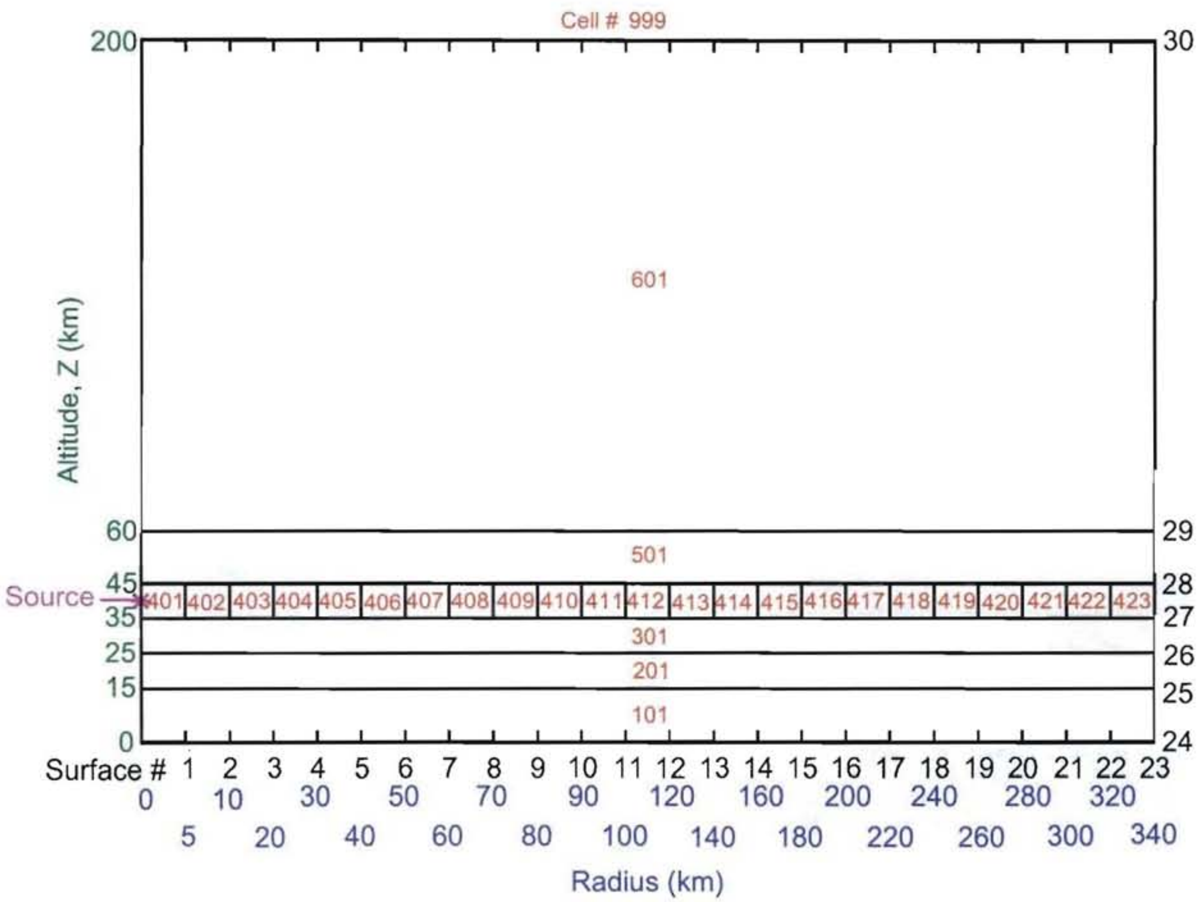

Figure 8: Spatial cell geometry for the co-altitude test problems with the modified here MCNP6.

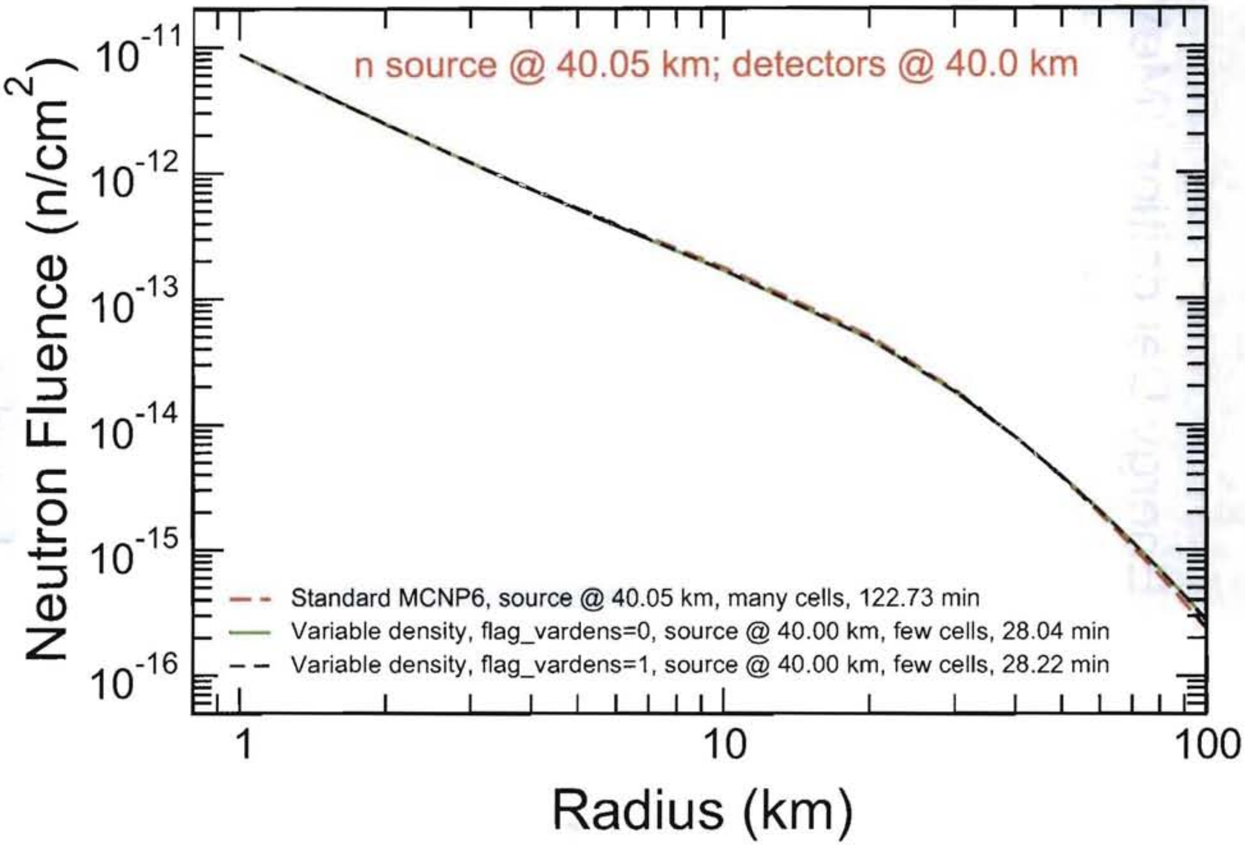

Figure 9: Neutron fluence at 40 km from a source at 40.00 km vs. radius (slant range) calculated with the modified here MCNP6 for the "reduced" geometry shown in Fig. 8 using the fixed Monti parameters for the density and mass-integral scale factors (solid green line; flag_vardens=0) and with the more universal X-3-MCC method (black dashed line; flag_vardens=1) compared with similar results by the unmodified MCNP6 with a source at 40.05 km and the "extended" geometry shown in Fig. 1 (red dashed line). The time needed for each version to run in a sequential mode 10^6 histories (nsp = 1000000) on a single Yellowrail node of the LANL Roadrunner supercomputer is shown in the legend.

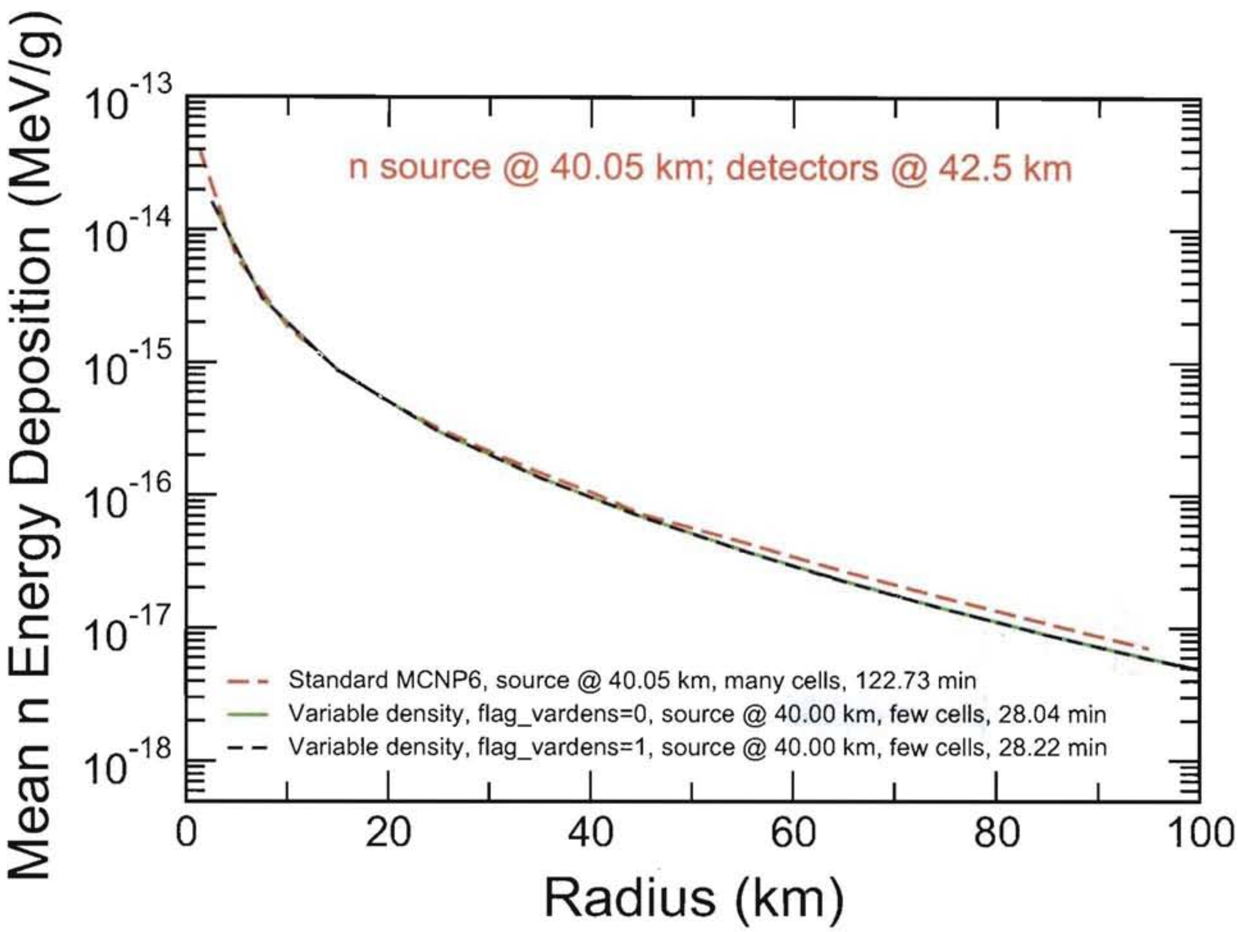

Figure 10: Mean neutron energy deposition at 40.0 km from a source at 40.00 km vs. radius (slant range) calculated with the modified here MCNP6 for the "reduced" geometry shown in Fig. 8 using the fixed Monti parameters for the density and mass-integral scale factors (solid green line; flag_vardens=0) and with the more universal X-3-MCC method (black dashed line; flag_vardens=1) compared with similar results by the unmodified MCNP6 with a source at 40.05 km and the "extended" geometry shown in Fig. 1 (red dashed line). The time needed for each version to run in a sequential mode 10^6 histories (nsp = 1000000) on a single Yellowrail node of the LANL Roadrunner supercomputer is shown in the legend.

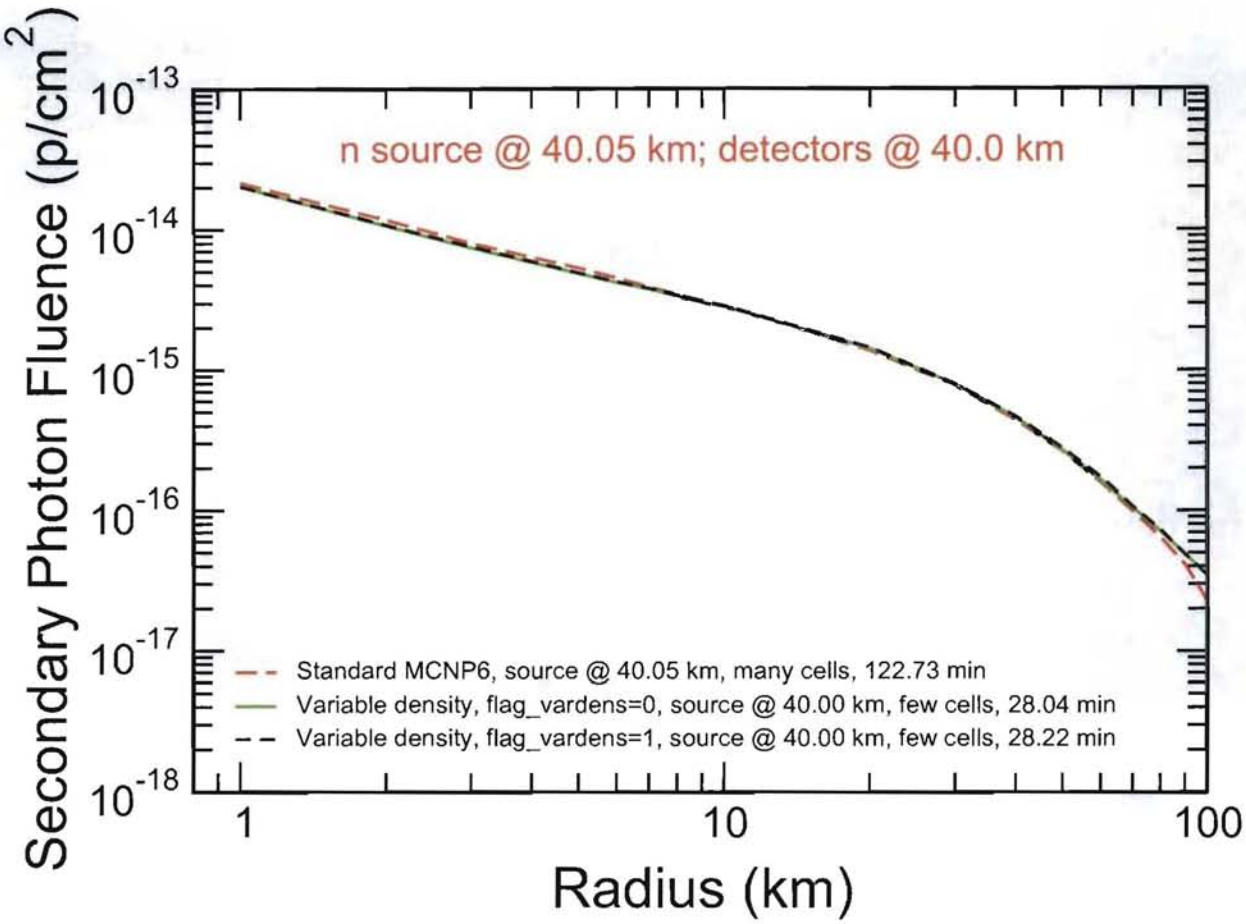

Figure 11: Secondary photon fluence at 40 km from a source at 40.00 km vs. radius (slant range) calculated with the modified here MCNP6 for the "reduced" geometry shown in Fig. 8 using the fixed Monti parameters for the density and mass-integral scale factors (solid green line; flag_vardens=0) and with the more universal X-3-MCC method (black dashed line; flag_vardens=1) compared with similar results by the unmodified MCNP6 with a source at 40.05 km and the "extended" geometry shown in Fig. 1 (red dashed line). The time needed for each version to run in a sequential mode 10^6 histories (nsp = 1000000) on a single Yellowrail node of the LANL Roadrunner supercomputer is shown in the legend.

REFERENCES

[1] Forrest B. Brown and William R. Martin, "Direct Sampling of Monte Carlo Flight Paths in Media with Continuously Varying Cross-Sections," *Proc. Nuclear Mathematical and Computational Sciences, ANS Mathematical and Computational Topical Meeting, Gatlinburg, TN, April 6-11, 2003*; LANL Report LA-UR-02-6530, Los Alamos, 2002.

[2] X-5 Monte Carlo Team, "MCNP – A General Monte Carlo N-Particle Transport Code, Version 5, Volume I: Overview and Theory," LANL Report LA-UR-03-1997, Los Alamos, 2003.

[3] E. R. Woodcock, T. Murphy, P. J. Hemmings, and T. C. Longworth, "Techniques Used in the GEM Code for Monte Carlo Neutronics Calculations in Reactors and Other Systems of Complex Geometry," *Proc. Conf. Applications of Computing Methods to Reactor Problems*, ANL-7050, p. 557, Argonne National Laboratory, 1965.

[4] C. J. Everett, E. D. Cashwell, and R. G. Schrandt, "A Monte Carlo Transport Routine for the "U. S. Standard Atmosphere" (1962) to an Altitude of 90 Kilometers," LASL Report LA-5089-MS, UC-34, Los Alamos, 1972.

[5] L. L. Carter, E. D. Cashwell, and W. M. Taylor, "Monte Carlo Sampling with Continuously Varying Cross Section Along Flight Paths," Nucl. Sci. Eng. **48** (1972) 403-4011.

[6] S. N. Cramer, "Application of the Fictitious Scattering Radiation Transport Model for Deep-Penetration Monte Carlo Calculations," ORNL Report ORNL/TM-48880, Oak Ridge, 1977.

[7] Forrest B. Brown and William R. Martin, "Direct Sampling of Monte Carlo Flight Paths in Media with Continuously Varying Cross-Sections," presentation (viewgraphs) at the NECDC 2002, October 21-24, 2002, Naval Postgraduate School, Monterey, CA, LANL Report LA-UR-02-6567, Los Alamos, 2002.

[8] Forrest Brown, David Griesheimer, and William Martin, "Continuously Varying Material Properties and Tallies for Monte Carlo Calculations," *Proc. PHYSOR-2004, ANS Reactor Physics Topical Meeting, Chicago, IL, April 25-29, 2004*, LANL Report LA-UR-04-0732, Los Alamos, 2004.

[9] Raymond A. Shulstad, "An Evaluation of Mass Integral Scaling as Applied to the Atmospheric Radiation Transport Problem," PhD thesis, Air Force Institute if Technology (AFIT/SA), Wright-Patterson AFB, OH, DS/PH/76-3, 1976.

[10] C. D. Zerby, "Radiation Flux Transformation as a Function of Density in an Infinite Medium with Anisotropic Point Sources," ORNL Report 2100, Oak Ridge, 1965.

[11] David L. Monti, "High Altitude Neutral Particle Transport Using the Monte Carlo Simulation Code MCNPX with Variable Density Atmosphere," Thesis, Air Force Institute of

Technology, AFIT/GNE/ENP/91M-6, Wright-Patterson Air Force Base, Ohio, March 1991.

[12] David L. Monti, "Modifications to MCNP, Version 3B: Incorporating a Variable Density Atmosphere," Air Force Institute of Technology Technical Report: AFIT/EN-TR-91-2, Wright-Patterson AFB, OH, March 1991.

[13] R. J. Harris, J. H. Lonergan, and L. Huszar, "Models of Radiation Transport in Air – The ATR Code," SAI-71-557-LJ, La Jolla, CA, Science Applications, Inc., May 1972.

[14] J. E. Campbell, S. A. Dupree, and M. L. Forsma, "CDR: A Program to Calculate Constant Dose Range from a Point Source of Radiation in the Atmosphere," NWEF 1081, Kirtland AFB, NM: Naval Weapons Effects Facility, 1971.

[15] Harry M. Murthy, "A User Guide to the SMAUG Computer Code," AFWL-TR-72-3, Air Force Weapon Laboratory, Kirtland AFB, NM, May 1972; "A User Guide to the SMAUG-II Computer Code," Air Force Weapon Laboratory, Kirtland AFB, NM, 4 March 1981.

[16] *U.S. Standard Atmosphere, 1976*, National Oceanic and Atmospheric Administration, National Aeronautics and Space Administration, United States Air Force, NOAA-S/T 76-1762, Washington, D.C., October 1976.

[17] Donald R. Culp, David L. Monti, James R. Shoemaker, David Wesley, and Kirk A. Mathews, "Monte Carlo Simulation of Atmospheric Neutron Transport at High Altitudes Using MCNP," AFIT Technical Report: AFIT/EN-TR-90-5, Wright-Patterson AFB, OH, August 1990.

Appendix 1

Example of an input used for test-problems with the unmodified MCNP6; to be able to compare our results with calculations by Monti, we use here exactly the same values for densities of cells as employed in Ref. [17]

```
Many cells, without vard cards, NPS=1000000,
C to test the flag_vardens = -1, i.e., the standard MCNP6 version
101  1 -6.770E-5  16 -17 -1       IMP:N=276    IMP:P=95
102  1 -6.770E-5  16 -17 1 -2     IMP:N=45.4   IMP:P=6.3
103  1 -6.770E-5  16 -17 2 -3     IMP:N=32.0   IMP:P=3.1
104  1 -6.770E-5  16 -17 3 -4     IMP:N=32.1   IMP:P=3.2
105  1 -6.770E-5  16 -17 4 -5     IMP:N=39.8   IMP:P=5
106  1 -6.770E-5  16 -17 5 -6     IMP:N=54.5   IMP:P=4.6
107  1 -6.770E-5  16 -17 6 -7     IMP:N=66.3   IMP:P=6.2
108  1 -6.770E-5  16 -17 7 -8     IMP:N=97.0   IMP:P=10.2
109  1 -6.770E-5  16 -17 8 -9     IMP:N=140    IMP:P=11.9
110  1 -6.770E-5  16 -17 9 -10    IMP:N=165    IMP:P=12.6
111  1 -6.770E-5  16 -17 10 -11   IMP:N=186    IMP:P=11.6
112  1 -6.770E-5  16 -17 11 -12   IMP:N=256    IMP:P=23.7
113  1 -6.770E-5  16 -17 12 -13   IMP:N=396    IMP:P=37.9
114  1 -6.770E-5  16 -17 13 -14   IMP:N=583    IMP:P=24.7
115  1 -6.770E-5  16 -17 14 -15   IMP:N=2309   IMP:P=71.1
201  1 -5.663E-5  17 -18 -1       IMP:N=127.4  IMP:P=40.6
202  1 -5.663E-5  17 -18 1 -2     IMP:N=21.5   IMP:P=4.5
203  1 -5.663E-5  17 -18 2 -3     IMP:N=15.6   IMP:P=2.1
204  1 -5.663E-5  17 -18 3 -4     IMP:N=15.7   IMP:P=2.3
205  1 -5.663E-5  17 -18 4 -5     IMP:N=18.9   IMP:P=2.9
206  1 -5.663E-5  17 -18 5 -6     IMP:N=27.6   IMP:P=2.9
207  1 -5.663E-5  17 -18 6 -7     IMP:N=34.9   IMP:P=3.8
208  1 -5.663E-5  17 -18 7 -8     IMP:N=50     IMP:P=5.9
209  1 -5.663E-5  17 -18 8 -9     IMP:N=71.5   IMP:P=6.9
210  1 -5.663E-5  17 -18 9 -10    IMP:N=78.4   IMP:P=7.4
211  1 -5.663E-5  17 -18 10 -11   IMP:N=90.8   IMP:P=9.2
212  1 -5.663E-5  17 -18 11 -12   IMP:N=140    IMP:P=17.2
213  1 -5.663E-5  17 -18 12 -13   IMP:N=216    IMP:P=21.9
214  1 -5.663E-5  17 -18 13 -14   IMP:N=324    IMP:P=19.6
215  1 -5.663E-5  17 -18 14 -15   IMP:N=1179   IMP:P=71.1
301  1 -4.349E-5  18 -19 -1       IMP:N=53.3   IMP:P=16.2
302  1 -4.349E-5  18 -19 1 -2     IMP:N=10.2   IMP:P=2.8
303  1 -4.349E-5  18 -19 2 -3     IMP:N=7.4    IMP:P=1.5
304  1 -4.349E-5  18 -19 3 -4     IMP:N=7.7    IMP:P=1.5
305  1 -4.349E-5  18 -19 4 -5     IMP:N=9.2    IMP:P=1.8
306  1 -4.349E-5  18 -19 5 -6     IMP:N=13.5   IMP:P=2.2
307  1 -4.349E-5  18 -19 6 -7     IMP:N=17.7   IMP:P=2.8
308  1 -4.349E-5  18 -19 7 -8     IMP:N=25.5   IMP:P=3.2
309  1 -4.349E-5  18 -19 8 -9     IMP:N=35.1   IMP:P=4.1
310  1 -4.349E-5  18 -19 9 -10    IMP:N=37.0   IMP:P=3.9
311  1 -4.349E-5  18 -19 10 -11   IMP:N=46.1   IMP:P=5.3
312  1 -4.349E-5  18 -19 11 -12   IMP:N=78.4   IMP:P=8.8
313  1 -4.349E-5  18 -19 12 -13   IMP:N=125    IMP:P=11.6
314  1 -4.349E-5  18 -19 13 -14   IMP:N=185    IMP:P=11.6
315  1 -4.349E-5  18 -19 14 -15   IMP:N=523    IMP:P=40.6
401  1 -3.043E-5  19 -20 -1       IMP:N=32.8   IMP:P=13.5
402  1 -3.043E-5  19 -20 1 -2     IMP:N=6.7    IMP:P=2.5
403  1 -3.043E-5  19 -20 2 -3     IMP:N=4.8    IMP:P=1.5
404  1 -3.043E-5  19 -20 3 -4     IMP:N=5.1    IMP:P=1.4
405  1 -3.043E-5  19 -20 4 -5     IMP:N=6.3    IMP:P=1.5
406  1 -3.043E-5  19 -20 5 -6     IMP:N=8.8    IMP:P=1.7
407  1 -3.043E-5  19 -20 6 -7     IMP:N=12.1   IMP:P=2.4
408  1 -3.043E-5  19 -20 7 -8     IMP:N=17.5   IMP:P=2.5
409  1 -3.043E-5  19 -20 8 -9     IMP:N=23.1   IMP:P=3.1
```

```
410  1 -3.043E-5  19 -20 9 -10    IMP:N=24.3  IMP:P=3.1
411  1 -3.043E-5  19 -20 10 -11   IMP:N=31.2  IMP:P=3.9
412  1 -3.043E-5  19 -20 11 -12   IMP:N=51.7  IMP:P=6.7
413  1 -3.043E-5  19 -20 12 -13   IMP:N=78.2  IMP:P=8.5
414  1 -3.043E-5  19 -20 13 -14   IMP:N=125   IMP:P=9.2
415  1 -3.043E-5  19 -20 14 -15   IMP:N=298   IMP:P=27.1
501  1 -2.129E-5  20 -21 -1       IMP:N=24.4  IMP:P=12.1
502  1 -2.129E-5  20 -21 1 -2     IMP:N=4.9   IMP:P=2.2
503  1 -2.129E-5  20 -21 2 -3     IMP:N=3.7   IMP:P=1.5
504  1 -2.129E-5  20 -21 3 -4     IMP:N=4.1   IMP:P=1.5
505  1 -2.129E-5  20 -21 4 -5     IMP:N=5.3   IMP:P=1.4
506  1 -2.129E-5  20 -21 5 -6     IMP:N=7.1   IMP:P=1.7
507  1 -2.129E-5  20 -21 6 -7     IMP:N=10    IMP:P=2.0
508  1 -2.129E-5  20 -21 7 -8     IMP:N=13.7  IMP:P=2.4
509  1 -2.129E-5  20 -21 8 -9     IMP:N=18    IMP:P=2.6
510  1 -2.129E-5  20 -21 9 -10    IMP:N=19.5  IMP:P=2.8
511  1 -2.129E-5  20 -21 10 -11   IMP:N=25.1  IMP:P=3.1
512  1 -2.129E-5  20 -21 11 -12   IMP:N=41.1  IMP:P=5.7
513  1 -2.129E-5  20 -21 12 -13   IMP:N=59.7  IMP:P=7.9
514  1 -2.129E-5  20 -21 13 -14   IMP:N=105   IMP:P=9
515  1 -2.129E-5  20 -21 14 -15   IMP:N=233   IMP:P=17.8
601  1 -1.266E-5  21 -22 -1       IMP:N=9.5   IMP:P=8.5
602  1 -1.266E-5  21 -22 1 -2     IMP:N=2.5   IMP:P=1.8
603  1 -1.266E-5  21 -22 2 -3     IMP:N=2.2   IMP:P=1.2
604  1 -1.266E-5  21 -22 3 -4     IMP:N=2.6   IMP:P=1.1
605  1 -1.266E-5  21 -22 4 -5     IMP:N=3.4   IMP:P=1.1
606  1 -1.266E-5  21 -22 5 -6     IMP:N=4.6   IMP:P=1.3
607  1 -1.266E-5  21 -22 6 -7     IMP:N=6.3   IMP:P=1.5
608  1 -1.266E-5  21 -22 7 -8     IMP:N=8.6   IMP:P=1.8
609  1 -1.266E-5  21 -22 8 -9     IMP:N=11.3  IMP:P=1.9
610  1 -1.266E-5  21 -22 9 -10    IMP:N=13.0  IMP:P=2.3
611  1 -1.266E-5  21 -22 10 -11   IMP:N=17.9  IMP:P=2.5
612  1 -1.266E-5  21 -22 11 -12   IMP:N=27.9  IMP:P=3.9
613  1 -1.266E-5  21 -22 12 -13   IMP:N=42.7  IMP:P=5.6
614  1 -1.266E-5  21 -22 13 -14   IMP:N=68.7  IMP:P=7.0
615  1 -1.266E-5  21 -22 14 -15   IMP:N=137   IMP:P=10.3
701  1 -6.187E-6  22 -23 -1       IMP:N=1.8   IMP:P=8.0
702  1 -6.187E-6  22 -23 1 -2     IMP:N=1.5   IMP:P=1.9
703  1 -6.187E-6  22 -23 2 -3     IMP:N=1.9   IMP:P=1.42
704  1 -6.187E-6  22 -23 3 -4     IMP:N=2.5   IMP:P=1.3
705  1 -6.187E-6  22 -23 4 -5     IMP:N=3.3   IMP:P=1.4
706  1 -6.187E-6  22 -23 5 -6     IMP:N=4.5   IMP:P=1.4
707  1 -6.187E-6  22 -23 6 -7     IMP:N=6     IMP:P=1.6
708  1 -6.187E-6  22 -23 7 -8     IMP:N=7.9   IMP:P=1.8
709  1 -6.187E-6  22 -23 8 -9     IMP:N=10.4  IMP:P=2.1
710  1 -6.187E-6  22 -23 9 -10    IMP:N=11.8  IMP:P=2.5
711  1 -6.187E-6  22 -23 10 -11   IMP:N=16.3  IMP:P=2.5
712  1 -6.187E-6  22 -23 11 -12   IMP:N=25.5  IMP:P=3.4
713  1 -6.187E-6  22 -23 12 -13   IMP:N=40.5  IMP:P=5
714  1 -6.187E-6  22 -23 13 -14   IMP:N=62.1  IMP:P=6.3
715  1 -6.187E-6  22 -23 14 -15   IMP:N=107   IMP:P=8.5
801  1 -3.034E-6  23 -24 -1       IMP:N=1     IMP:P=8.2
802  1 -3.034E-6  23 -24 1 -2     IMP:N=1.5   IMP:P=2.2
803  1 -3.034E-6  23 -24 2 -3     IMP:N=2.0   IMP:P=1.7
804  1 -3.034E-6  23 -24 3 -4     IMP:N=2.6   IMP:P=1.6
805  1 -3.034E-6  23 -24 4 -5     IMP:N=3.5   IMP:P=1.7
806  1 -3.034E-6  23 -24 5 -6     IMP:N=4.5   IMP:P=1.7
807  1 -3.034E-6  23 -24 6 -7     IMP:N=5.7   IMP:P=1.9
808  1 -3.034E-6  23 -24 7 -8     IMP:N=7.4   IMP:P=2.2
809  1 -3.034E-6  23 -24 8 -9     IMP:N=9.4   IMP:P=2.5
810  1 -3.034E-6  23 -24 9 -10    IMP:N=10.8  IMP:P=2.4
811  1 -3.034E-6  23 -24 10 -11   IMP:N=14.4  IMP:P=2.5
812  1 -3.034E-6  23 -24 11 -12   IMP:N=22.6  IMP:P=3.6
813  1 -3.034E-6  23 -24 12 -13   IMP:N=33.1  IMP:P=5
```

```
814  1 -3.034E-6  23 -24 13 -14   IMP:N=48.4  IMP:P=6.5
815  1 -3.034E-6  23 -24 14 -15   IMP:N=80.9  IMP:P=8.6
901  1 -1.485E-6  24 -25 -1       IMP:N=13.5  IMP:P=19
902  1 -1.485E-6  24 -25 1 -2     IMP:N=3.3   IMP:P=3.8
903  1 -1.485E-6  24 -25 2 -3     IMP:N=2.9   IMP:P=2.6
904  1 -1.485E-6  24 -25 3 -4     IMP:N=3.3   IMP:P=2.1
905  1 -1.485E-6  24 -25 4 -5     IMP:N=4     IMP:P=2.1
906  1 -1.485E-6  24 -25 5 -6     IMP:N=5     IMP:P=1.8
907  1 -1.485E-6  24 -25 6 -7     IMP:N=6.2   IMP:P=2.0
908  1 -1.485E-6  24 -25 7 -8     IMP:N=7.7   IMP:P=2.1
909  1 -1.485E-6  24 -25 8 -9     IMP:N=9.6   IMP:P=2.6
910  1 -1.485E-6  24 -25 9 -10    IMP:N=10.8  IMP:P=2.5
911  1 -1.485E-6  24 -25 10 -11   IMP:N=13.4  IMP:P=2.6
912  1 -1.485E-6  24 -25 11 -12   IMP:N=19.8  IMP:P=3.6
913  1 -1.485E-6  24 -25 12 -13   IMP:N=28.9  IMP:P=4.4
914  1 -1.485E-6  24 -25 13 -14   IMP:N=43.7  IMP:P=6
915  1 -1.485E-6  24 -25 14 -15   IMP:N=70.6  IMP:P=8.6
1001 1 -5.415E-7  25 -26 -1       IMP:N=34.6  IMP:P=31.6
1002 1 -5.415E-7  25 -26 1 -2     IMP:N=6.2   IMP:P=5.6
1003 1 -5.415E-7  25 -26 2 -3     IMP:N=3.8   IMP:P=2.8
1004 1 -5.415E-7  25 -26 3 -4     IMP:N=3.3   IMP:P=2
1005 1 -5.415E-7  25 -26 4 -5     IMP:N=3.4   IMP:P=2
1006 1 -5.415E-7  25 -26 5 -6     IMP:N=3.7   IMP:P=1.8
1007 1 -5.415E-7  25 -26 6 -7     IMP:N=4.2   IMP:P=1.8
1008 1 -5.415E-7  25 -26 7 -8     IMP:N=4.8   IMP:P=1.8
1009 1 -5.415E-7  25 -26 8 -9     IMP:N=5.6   IMP:P=1.8
1010 1 -5.415E-7  25 -26 9 -10    IMP:N=6.2   IMP:P=1.7
1011 1 -5.415E-7  25 -26 10 -11   IMP:N=7.5   IMP:P=1.8
1012 1 -5.415E-7  25 -26 11 -12   IMP:N=10.3  IMP:P=2.2
1013 1 -5.415E-7  25 -26 12 -13   IMP:N=14.2  IMP:P=2.7
1014 1 -5.415E-7  25 -26 13 -14   IMP:N=19.9  IMP:P=13.6
1015 1 -5.415E-7  25 -26 14 -15   IMP:N=27.8  IMP:P=14.6
1101 1 -8.038E-8  26 -27 -1       IMP:N=86.4  IMP:P=81.3
1102 1 -8.038E-8  26 -27 1 -3     IMP:N=6.9   IMP:P=4.6
1103 1 -8.038E-8  26 -27 3 -5     IMP:N=3.6   IMP:P=1.9
1104 1 -8.038E-8  26 -27 5 -7     IMP:N=3.1   IMP:P=1.4
1105 1 -8.038E-8  26 -27 7 -9     IMP:N=3.2   IMP:P=1.3
1106 1 -8.038E-8  26 -27 9 -11    IMP:N=3.3   IMP:P=1.1
1107 1 -8.038E-8  26 -27 11 -13   IMP:N=4.6   IMP:P=1.2
1108 1 -8.038E-8  26 -27 13 -15   IMP:N=7.3   IMP:P=1.7
1201 1 -4.619E-9  27 -28 -1       IMP:N=299   IMP:P=114
1202 1 -4.619E-9  27 -28 1 -3     IMP:N=19.2  IMP:P=11.2
1203 1 -4.619E-9  27 -28 3 -5     IMP:N=8.3   IMP:P=4.7
1204 1 -4.619E-9  27 -28 5 -7     IMP:N=5.9   IMP:P=2.8
1205 1 -4.619E-9  27 -28 7 -9     IMP:N=5     IMP:P=2.0
1206 1 -4.619E-9  27 -28 9 -11    IMP:N=3.9   IMP:P=1.4
1207 1 -4.619E-9  27 -28 11 -13   IMP:N=4.3   IMP:P=1.4
1208 1 -4.619E-9  27 -28 13 -15   IMP:N=5.7   IMP:P=1.6
1301 2 -8.013E-12 28 -29 -1       IMP:N=508   IMP:P=190
1302 2 -8.013E-12 28 -29 1 -5     IMP:N=12.8  IMP:P=7.0
1303 2 -8.013E-12 28 -29 5 -9     IMP:N=5.2   IMP:P=2.3
1304 2 -8.013E-12 28 -29 9 -12    IMP:N=3.3   IMP:P=1.2
1305 2 -8.013E-12 28 -29 12 -15   IMP:N=3.1   IMP:P=1
1401 3 -6.439E-14 29 -30 -1       IMP:N=1847  IMP:P=569
1402 3 -6.439E-14 29 -30 1 -5     IMP:N=37.6  IMP:P=19.6
1403 3 -6.439E-14 29 -30 5 -9     IMP:N=13.6  IMP:P=15.6
1404 3 -6.439E-14 29 -30 9 -12    IMP:N=6.6   IMP:P=2.7
1405 3 -6.439E-14 29 -30 12 -15   IMP:N=4.9   IMP:P=1.7
1501 4 -3.187E-15 30 -31 -1       IMP:N=2770  IMP:P=569
1502 4 -3.187E-15 30 -31 1 -5     IMP:N=72.7  IMP:P=43.2
1503 4 -3.187E-15 30 -31 5 -9     IMP:N=25.5  IMP:P=9.5
1504 4 -3.187E-15 30 -31 9 -12    IMP:N=10.7  IMP:P=4.2
1505 4 -3.187E-15 30 -31 12 -15   IMP:N=6.8   IMP:P=2.6
999  0    31:-16:15               IMP:N=0     IMP:P=0       $ OUTSIDE WORLD
```

```
C 15  CONCENTRIC CYLINDERS 16 PLANES PERPENDICULAR TO Z AXIS
1  CZ   2.5E+5
2  CZ   7.5E+5
3  CZ  12.5E+5
4  CZ  17.5E+5
5  CZ  22.5E+5
6  CZ  27.5E+5
7  CZ  32.5E+5
8  CZ  37.5E+5
9  CZ  42.5E+5
10 CZ  50.0E+5
11 CZ  60.0E+5
12 CZ  70.0E+5
13 CZ  80.0E+5
14 CZ  90.0E+5
15 CZ 100.0E+5
16 PZ  20.0E+5
17 PZ 21.25E+5
18 PZ  22.5E+5
19 PZ  25.0E+5
20 PZ  27.5E+5
21 PZ  30.0E+5
22 PZ  35.0E+5
23 PZ  40.0E+5
24 PZ  45.0E+5
25 PZ  50.0E+5
26 PZ  60.0E+5
27 PZ  80.0E+5
28 PZ 100.0E+5
29 PZ 150.0E+5
30 PZ 200.0E+5
31 PZ 300.0E+5

MODE  N P
C     ISOTROPIC FISSION SOURCE AT (0,0,50 klicks)
SDEF  ERG=D1 POS=0 0 40.05E+5 CEL=801
SC1  FISSION SPECTRUM (GENERIC)
SI1  H 4.14E-7 1.1254E-6 3.059E-6 1.0677E-5 2.9023E-5 1.013E-4 5.8295E-4
        1.2341E-3 3.3546E-3 1.0333E-2 2.1875E-2 2.4788E-2 5.2475E-2
        0.1111 0.1576 0.5502 1.108 1.827 2.307 2.385
        3.012 4.066 4.724 4.966 6.376 7.408 8.187
        9.048 10.00 11.05 12.21 12.82 13.84 14.19
SP1  D 0 0 0 0 0 2.0226E-3 2.3974E-2
        4.2300E-2 7.9823E-2 1.1337E-1 8.4647E-2 1.4145E-2 8.1805E-2
        7.0979E-2 3.3869E-2 9.8584E-2 8.4961E-2 6.2051E-2 2.5916E-2 3.6882E-3
        2.2402E-2 2.6063E-2 1.2918E-2 4.0545E-3 1.8073E-2 8.6953E-3 5.8951E-3
        6.1457E-3 7.8970E-3 9.4915E-3 1.6382E-2 1.7368E-2 3.3667E-2 9.3298E-3
C       MATERIAL SPECIFICATION
M1      7014.50D -0.78 $ DISCRETE NITROGEN XSEC
        8016.50D -0.22 $ DISCRETE OXYGEN XSEC
M2      7014.50D -0.78 $ DISCRETE NI'ROGEN XSEC
        8016.50D -0.22 $ DISCRETE OXYGEN XSEC
M3      7014.50D -0.78 $ DISCRETE NITROGEN XSEC
        8016.50D -0.22 $ DISCRETE OXYGEN XSEC
M4      7014.50D -0.78 $ DISCRETE NITROGEN XSEC
        8016.50D -0.22 $ DISCRETE OXYGEN XSEC
C       18000.35D -0.01 $ omitted don't have Ar Xsec with gammas!!!
PHYS:N,P 14.2 $ CROSS SECTIONS ABOVE 14.2 MEV WILL BE EXPUNGED.
C
C TALLY CARDS
C Energy deposition calculation for neutrons at 42.5 km altitude
F6:n 801 $ Energy deposition of neutrons in the cell #801
F16:n  802
```

```
F26:n  803
F36:n  804
F46:n  805
F56:n  806
F66:n  807
F76:n  808
F86:n  809
F96:n  810
F106:n 811
F116:n 812
F126:n 813
F136:n 814
F146:n 815
C neutron flux (1/cm2) from ring detector
C at 40 km altitude
F5Z:n     40.00E5   1.00E5 0.1E5 $ n flux for R = 1 km at Z=40 km altitude
F15Z:n    40.00E5   2.00E5 0.1E5
F25Z:n    40.00E5   3.00E5 0.1E5
F35Z:n    40.00E5   4.00E5 0.1E5
F45Z:n    40.00E5   5.00E5 0.1E5
F55Z:n    40.00E5   6.00E5 0.1E5
F65Z:n    40.00E5   7.00E5 0.1E5
F75Z:n    40.00E5   8.00E5 0.1E5
F85Z:n    40.00E5   9.00E5 0.1E5
F95Z:n    40.00E5  10.00E5 0.1E5
F105Z:n   40.00E5  20.00E5 0.1E5
F115Z:n   40.00E5  30.00E5 0.1E5
F125Z:n   40.00E5  40.00E5 0.1E5
F135Z:n   40.00E5  50.00E5 0.1E5
F145Z:n   40.00E5  60.00E5 0.1E5
F155Z:n   40.00E5  70.00E5 0.1E5
F165Z:n   40.00E5  80.00E5 0.1E5
F175Z:n   40.00E5  90.00E5 0.1E5
F185Z:n   40.00E5 100.00E5 0.1E5
C photon  flux (1/cm2) from ring detector
C at 40 km altitude
F205Z:p   40.00E5   1.00E5 0.1E5 $ photon flux for R = 1 km at Z=40 km altitude
F215Z:p   40.00E5   2.00E5 0.1E5
F225Z:p   40.00E5   3.00E5 0.1E5
F235Z:p   40.00E5   4.00E5 0.1E5
F245Z:p   40.00E5   5.00E5 0.1E5
F255Z:p   40.00E5   6.00E5 0.1E5
F265Z:p   40.00E5   7.00E5 0.1E5
F275Z:p   40.00E5   8.00E5 0.1E5
F285Z:p   40.00E5   9.00E5 0.1E5
F295Z:p   40.00E5  10.00E5 0.1E5
F305Z:p   40.00E5  20.00E5 0.1E5
F315Z:p   40.00E5  30.00E5 0.1E5
F325Z:p   40.00E5  40.00E5 0.1E5
F335Z:p   40.00E5  50.00E5 0.1E5
F345Z:p   40.00E5  60.00E5 0.1E5
F355Z:p   40.00E5  70.00E5 0.1E5
F365Z:p   40.00E5  80.00E5 0.1E5
F375Z:p   40.00E5  90.00E5 0.1E5
F385Z:p   40.00E5 100.00E5 0.1E5
C
F2:n 31 $ LEAKAGE OUT OF THE TOP SURFACE
C
NPS 1000000 $ RUN 1000000 HISTORIES
```

Appendix 2

Example of an input for test-problems with the variable density modification of MCNP6 using both **vard** and **varda** cards, i.e., invoking the X-3-MCC method

```
Few cells, NPS=1000000,
c using both vard and varda cards, i.e., using the X-3-MCC method
C Cell cards
101  1 -1.225E-3  24 -25 -23    IMP:N=1      IMP:P=1  $ Cell #101
201  1 -1.225E-3  25 -26 -23    IMP:N=1      IMP:P=1
301  1 -1.225E-3  26 -27 -23    IMP:N=1      IMP:P=1
401  1 -1.225E-3  27 -28 -1     IMP:N=1      IMP:P=1
402  1 -1.225E-3  27 -28 1 -2   IMP:N=1.21   IMP:P=1
403  1 -1.225E-3  27 -28 2 -3   IMP:N=1.44   IMP:P=1
404  1 -1.225E-3  27 -28 3 -4   IMP:N=2.4    IMP:P=1
405  1 -1.225E-3  27 -28 4 -5   IMP:N=4.08   IMP:P=1
406  1 -1.225E-3  27 -28 5 -6   IMP:N=6.75   IMP:P=1
407  1 -1.225E-3  27 -28 6 -7   IMP:N=10.3   IMP:P=2
408  1 -1.225E-3  27 -28 7 -8   IMP:N=15.54  IMP:P=2
409  1 -1.225E-3  27 -28 8 -9   IMP:N=20.6   IMP:P=3
410  1 -1.225E-3  27 -28 9 -10  IMP:N=29.85  IMP:P=3
411  1 -1.225E-3  27 -28 10 -11 IMP:N=40.6   IMP:P=3
412  1 -1.225E-3  27 -28 11 -12 IMP:N=40     IMP:P=5
413  1 -1.225E-3  27 -28 12 -13 IMP:N=58.8   IMP:P=5
414  1 -1.225E-3  27 -28 13 -14 IMP:N=89.6   IMP:P=8
415  1 -1.225E-3  27 -28 14 -15 IMP:N=318.1  IMP:P=8
416  1 -1.225E-3  27 -28 15 -16 IMP:N=340.8  IMP:P=8
417  1 -1.225E-3  27 -28 16 -17 IMP:N=449    IMP:P=10
418  1 -1.225E-3  27 -28 17 -18 IMP:N=637    IMP:P=15
419  1 -1.225E-3  27 -28 18 -19 IMP:N=1000   IMP:P=40
420  1 -1.225E-3  27 -28 19 -20 IMP:N=1      IMP:P=1
421  1 -1.225E-3  27 -28 20 -21 IMP:N=1      IMP:P=1
422  1 -1.225E-3  27 -28 21 -22 IMP:N=1      IMP:P=1
423  1 -1.225E-3  27 -28 22 -23 IMP:N=1      IMP:P=1
501  1 -1.225E-3  28 -29 -23    IMP:N=1      IMP:P=1
601  1 -1.225E-3  29 -30 -23    IMP:N=1      IMP:P=1
999  0            23:-24:30     IMP:N=0      IMP:P=0       $ Outside world (void)

C Surface cards
C 23  CONCENTRIC CYLINDERS and 7 PLANES PERPENDICULAR TO Z-AXIS
1  CZ  5E+5 $ Surface # 1
2  CZ  10E+5
3  CZ  20E+5
4  CZ  30E+5
5  CZ  40E+5
6  CZ  50E+5
7  CZ  60E+5
8  CZ  70E+5
9  CZ  80E+5
10 CZ  90E+5
11 CZ  100E+5
12 CZ  120E+5
13 CZ  140E+5
14 CZ  160E+5
15 CZ  180E+5
16 CZ  200E+5
17 CZ  220E+5
18 CZ  240E+5
19 CZ  260E+5
20 CZ  280E+5
21 CZ  300E+5
22 CZ  320E+5
```

```
23 CZ  340E+5
24 PZ  0
25 PZ  15E+5
26 PZ  25E+5
27 PZ  35E+5
28 PZ  45E+5
29 PZ  60E+5
30 PZ  200E+5

MODE  N P
C     ISOTROPIC NEUTRON SOURCE AT (0,0,40 klicks)
SDEF  ERG=D1 POS=0 0 40E+5 CEL=401
SC1   SOURCE SPECTRUM (GENERIC)
SI1   H 4.14E-7 1.1254E-6 3.059E-6 1.0677E-5 2.9023E-5 1.013E-4 5.8295E-4
        1.2341E-3 3.3546E-3 1.0333E-2 2.1875E-2 2.4788E-2 5.2475E-2
        0.1111 0.1576 0.5502 1.108 1.827 2.307 2.385
        3.012 4.066 4.724 4.966 6.376 7.408 8.187
        9.048 10.00 11.05 12.21 12.82 13.84 14.19
SP1   D 0 0 0 0 0 2.0226E-3 2.3974E-2
        4.2300E-2 7.9823E-2 1.1337E-1 8.4647E-2 1.4145E-2 8.1805E-2
        7.0979E-2 3.3869E-2 9.8584E-2 8.4961E-2 6.2051E-2 2.5916E-2 3.6882E-3
        2.2402E-2 2.6063E-2 1.2918E-2 4.0545E-3 1.8073E-2 8.6953E-3 5.8951E-3
        6.1457E-3 7.8970E-3 9.4915E-3 1.6382E-2 1.7368E-2 3.3667E-2 9.3298E-3
C       MATERIAL SPECIFICATION
M1    7014.50D -0.78 $ DISCRETE NITROGEN XSEC
        8016.50D -0.22 $ DISCRETE OXYGEN XSEC
PHYS:N,P 14.2 $ CROSS SECTIONS ABOVE 14.2 MEV WILL BE EXPUNGED.
C
C TALLY CARDS
C Energy deposition calculation for neutrons at 40.0 km altitude
F6:n   401 $ Energy deposition of neutrons in the cell #401
F16:n  402
F26:n  403
F36:n  404
F46:n  405
F56:n  406
F66:n  407
F76:n  408
F86:n  409
F96:n  410
F106:n 411
F116:n 412
F126:n 413
F136:n 414
F146:n 415
F156:n 416
F166:n 417
F176:n 418
F186:n 419
F196:n 420
F206:n 421
F216:n 422
F226:n 423
C neutron flux (1/cm2) from ring detector
C at 40 km altitude
F5Z:n    40.00E5  1.00E5 0.1E5 $ n flux for R = 1 km at Z=40 km altitude
F15Z:n   40.00E5  2.00E5 0.1E5
F25Z:n   40.00E5  3.00E5 0.1E5
F35Z:n   40.00E5  4.00E5 0.1E5
F45Z:n   40.00E5  5.00E5 0.1E5
F55Z:n   40.00E5  6.00E5 0.1E5
F65Z:n   40.00E5  7.00E5 0.1E5
F75Z:n   40.00E5  8.00E5 0.1E5
F85Z:n   40.00E5  9.00E5 0.1E5
```

```
F95Z:n   40.00E5 10.00E5 0.1E5
F105Z:n  40.00E5 20.00E5 0.1E5
F115Z:n  40.00E5 30.00E5 0.1E5
F125Z:n  40.00E5 40.00E5 0.1E5
F135Z:n  40.00E5 50.00E5 0.1E5
F145Z:n  40.00E5 60.00E5 0.1E5
F155Z:n  40.00E5 70.00E5 0.1E5
F165Z:n  40.00E5 80.00E5 0.1E5
F175Z:n  40.00E5 90.00E5 0.1E5
F185Z:n  40.00E5 100.00E5 0.1E5
C photon  flux (1/cm2) from ring detector
C at 40 km altitude
F205Z:p  40.00E5  1.00E5 0.1E5 $ photon flux for R = 1 km at Z=40 km altitude
F215Z:p  40.00E5  2.00E5 0.1E5
F225Z:p  40.00E5  3.00E5 0.1E5
F235Z:p  40.00E5  4.00E5 0.1E5
F245Z:p  40.00E5  5.00E5 0.1E5
F255Z:p  40.00E5  6.00E5 0.1E5
F265Z:p  40.00E5  7.00E5 0.1E5
F275Z:p  40.00E5  8.00E5 0.1E5
F285Z:p  40.00E5  9.00E5 0.1E5
F295Z:p  40.00E5 10.00E5 0.1E5
F305Z:p  40.00E5 20.00E5 0.1E5
F315Z:p  40.00E5 30.00E5 0.1E5
F325Z:p  40.00E5 40.00E5 0.1E5
F335Z:p  40.00E5 50.00E5 0.1E5
F345Z:p  40.00E5 60.00E5 0.1E5
F355Z:p  40.00E5 70.00E5 0.1E5
F365Z:p  40.00E5 80.00E5 0.1E5
F375Z:p  40.00E5 90.00E5 0.1E5
F385Z:p  40.00E5 100.00E5 0.1E5
C     Variable density input cards
vard vdalpha 0.e0 vdbeta  0.e0 vdgamma 1.e0
varda     0.0       1.2250e-3
        1.0e+5      1.1117e-3
        2.0e+5      1.0066e-3
        3.0e+5      9.0925e-4
        4.0e+5      8.1935e-4
        5.0e+5      7.3643e-4
        1.0e+6      4.1351e-4
        1.5e+6      1.9476e-4
        2.0e+6      8.8910e-5
        2.5e+6      4.0084e-5
        3.0e+6      1.8410e-5
        4.0e+6      3.9957e-6
        5.0e+6      1.0269e-6
        6.0e+6      3.0968e-7
        7.0e+6      8.2829e-8
        8.0e+6      1.8458e-8
        9.0e+6      3.4160e-9
        1.0e+7      5.604e-10
        1.1e+7      9.708e-11
        1.2e+7      2.222e-11
        1.3e+7      8.152e-12
        1.4e+7      3.831e-12
        1.5e+7      2.076e-12
        1.6e+7      1.233e-12
        1.8e+7      5.194e-13
        2.0e+7      2.541e-13
        2.4e+7      7.858e-14
        2.8e+7      2.971e-14
        3.2e+7      1.264e-14
        4.0e+7      2.803e-15
        4.8e+7      7.208e-16
```

```
     5.6e+7     2.049e-16
     6.4e+7     6.523e-17
     7.2e+7     2.448e-17
     8.0e+7     1.136e-17
     8.8e+7     6.464e-18
     9.9e+7     3.716e-18
     1.0e+8     3.561e-18
C
NPS 1000000 $ RUN 1000000 HISTORIES
```

SGM:sgm

Distribution:

Eolus Team
B. J. Archer, X-3, F644
D. L. Crane, W-13, T080
S. S. McCready, W-13, T080
K. C. Kelley, W-13, T080
G. W. McKinney, D-5, K575
L. S. Waters, D-5, K575
M. R. James, D-5, K575
X-DO file
W-DO file
X-3 file